A strontium isoscape of northern Australia

Patrice de Caritat[1], Anthony Dosseto[2], Florian Dux[2]

[1]Geoscience Australia, GPO Box 378, Canberra ACT 2601, Australia
[2]Wollongong Isotope Geochronology Laboratory, School of Earth, Atmospheric and Life Sciences, University of
Wollongong, Wollongong NSW 2522, Australia

Correspondence to: Patrice de Caritat (Patrice.deCaritat@ga.gov.au)

Abstract

Strontium isotopes ($^{87}Sr/^{86}Sr$) are useful to trace processes in the Earth sciences as well as in forensic, archaeological, palaeontological, and ecological sciences. As very few large-scale Sr isoscapes exist in Australia, we have identified an opportunity to determine $^{87}Sr/^{86}Sr$ ratios on archived fluvial sediment samples from the low-density National Geochemical Survey of Australia. The present study targeted the northern parts of Western Australia, the Northern Territory and Queensland, north of 21.5 °S. The samples were taken mostly from a depth of ~60-80 cm in floodplain deposits at or near the outlet of large catchments (drainage basins). A coarse (< 2 mm) grain-size fraction was air-dried, sieved, milled then digested (hydrofluoric acid + nitric acid followed by aqua regia) to release *total* Sr. The Sr was then separated by chromatography and the $^{87}Sr/^{86}Sr$ ratio determined by multicollector-inductively coupled plasma mass spectrometry. Results demonstrate a wide range of Sr isotopic values (0.7048 to 1.0330) over the survey area, reflecting a large diversity of source rock lithologies, geological processes and bedrock ages. Spatial distribution of $^{87}Sr/^{86}Sr$ shows coherent (multi-point anomalies and smooth gradients), large-scale (> 100 km) patterns that appear to be broadly consistent with surface geology, regolith/soil type, and/or nearby outcropping bedrock. For instance, the extensive black clay soils of the Barkly Tableland define a > 500 km-long northwest-southeast-trending unradiogenic anomaly ($^{87}Sr/^{86}Sr$ < 0.7182). Where sedimentary carbonate or mafic/ultramafic igneous rocks dominate, low to moderate $^{87}Sr/^{86}Sr$ values are generally recorded (medians of 0.7387 and 0.7422, respectively). In proximity to the outcropping Proterozoic metamorphic basement of the Tennant, McArthur, Murphy and Mount Isa geological regions, conversely, radiogenic $^{87}Sr/^{86}Sr$ values (> 0.7655) are observed. A potential correlation between mineralisation and elevated $^{87}Sr/^{86}Sr$ values in these regions needs to be investigated in greater detail. Our results to-date indicate that incorporating soil/regolith Sr isotopes in regional, exploratory geoscience investigations can help identify basement rock types under (shallow) cover, constrain surface processes (for instance weathering, dispersion), and, potentially, recognise components of mineral systems. Furthermore, the resulting Sr isoscape and future models derived therefrom can also be utilised in forensic, archaeological, paleontological and ecological studies that aim to investigate, e.g. past and modern animal (including humans) dietary habits and migrations. The new spatial Sr isotope dataset for the northern Australia region is publicly available (de Caritat et al., 2022a; https://dx.doi.org/10.26186/147473).

1 Introduction

Strontium isotope ratios ($^{87}Sr/^{86}Sr$) can be measured in many geological materials as the trace element strontium (Sr) is relatively abundant and readily substitutes for calcium (Ca) in minerals and organic tissues. The $^{87}Sr/^{86}Sr$ of a mineral or rock is a function of (1) its initial and unchanging ^{86}Sr content, (2) its initial rubidium (Rb) content (thus Rb/Sr ratio), and (3) time (e.g. McNutt, 2000). Rubidium substitutes readily for potassium (K) in minerals and is thus relatively common too. As one of the two naturally occurring Rb isotopes, ^{87}Rb, which accounts to 27.8 % of Rb, decays over time (by emitting a negative beta particle) to stable ^{87}Sr ($t_{1/2}$ = 49.6 x 10^9 years), the $^{87}Sr/^{86}Sr$ ratio of that material slowly increases with time (e.g. Rotenberg et al., 2012; Nebel and Stammeier, 2018). During geological processes such as mineral dissolution or precipitation, or biological processes such as bone and tooth growth, the $^{87}Sr/^{86}Sr$ remains constant as there is no fractionation (e.g. Gosz et al., 1983; Nebel and Stammeier, 2018). These characteristics make the Sr isotopic system very useful in the geosciences, where it has been used for decades for instance in the study of

• sediment diagenesis and low-grade metamorphism (e.g. Swart et al., 1987; Schultz et al., 1989; Mountjoy et al., 1992; Schaltegger et al., 1994),

• sediment, dust and soil provenance (e.g. Douglas et al., 1995; Revel-Rolland et al., 2006; Bathgate et al., 2011; Bataille and Bowen, 2012; De Deckker et al., 2014; Jomori et al., 2017; De Deckker, 2020; de Caritat et al., 2022b),

• stratigraphy and reservoir/basin analysis (e.g. Rundberg and Smalley, 1989; Smalley et al., 1989, 1992; McArthur et al., 2012),

• fluid flow (e.g. McNutt et al., 1987; Stueber et al., 1987; Sullivan et al., 1990; Bagheri et al., 2014),

• weathering and pedogenesis (e.g. Åberg et al., 1989; Faure and Felder, 1981; Wickman and Jacks, 1992; Blum et al., 1994; Bullen et al., 1994, 1997; Quade et al., 1995; Probst et al., 2000; Harrington and Herczeg, 2003; Oliver et al., 2003; Green et al., 2004),

• terrestrial ecosystems and catchment processes (e.g. Graustein, 1989; Jacks et al., 1989; Lyons et al., 1995; Négrel and Grosbois, 1999; Négrel and Pauwels, 2004; Gosselin et al., 2004; Chadwick et al, 2009; Hagedorn et al., 2011),

• hydrology and hydrogeology (e.g. Collerson et al., 1988; Andersson et al., 1992, 1994; Douglas et al., 1995; Yang et al., 1996; Grobe et al., 2000; Dogramaci and Herczeg, 2002; Ojiambo et al., 2003; Palmer et al., 2004; Cartwright et al., 2007; Christensen et al., 2018; Shin et al., 2021),

• environment and environmental change (e.g. Andersson et al., 1990; Åberg, 1995; Åberg et al., 1995; Oishi, 2021),

• (palaeo)climatology and palaeogeographic reconstructions (e.g. Blum and Erel, 1995; Wei et al., 2018; Flecker et al., 2002),

• determining the $^{87}Sr/^{86}Sr$ of seawater through geological time (e.g. Veizer, 1989; Gruszczynski et al., 1992; Denison et al., 1994a, 1994b; Shields, 2007), and

• ore genesis and mineral exploration (e.g. Le Bas et al., 1997; de Caritat et al., 2005; Daneshvar et al., 2020; Wei et al., 2020; Zhao et al., 2021).

65 Outside of the geosciences, food tracing and provenancing have also been underpinned by the use of Sr isotopes, though in this case relying generally on the *bioavailable* Sr rather than total Sr (e.g. Voerkelius et al., 2010; Di Paola-Naranjo et al., 2011; Vinciguerra et al., 2015; Hoogewerff et al., 2019; Moffat et al., 2020). Anthropological studies have relied on $^{87}Sr/^{86}Sr$ isotope ratios to locate archaeological artefacts or reconstruct ancient human behaviours (e.g. Frei and Frei, 2013; Willmes et al., 2014, 2018; Adams et al., 2019; Pacheco-Forés et al., 2020; Washburn et al., 2021). Animal migration studies have also

70 relied on Sr isotope data (e.g. Price et al., 2017). More recently, large-scale compilations and machine-learned predictions of the $^{87}Sr/^{86}Sr$ variations up to the continental and even global scale have been proposed (e.g. Bataille et al., 2014, 2018, 2020). Strontium isotope landscape maps ('isoscapes') provide the fundamental context required for the interpretation of more detailed scientific research about processes or provenance. Despite the plethora of research using Sr isotopes to address various scientific questions, very few Sr isoscapes exist in the southern hemisphere, particularly for soils or covering large

75 swathes of the Earth's surface (see Bataille et al., 2020). Two exceptions to this are (1) the work by Adams et al. (2019), which reported $^{87}Sr/^{86}Sr$ in plant, soil, and biota over ~300 000 km^2 on the Cape York Peninsula in Australia; and (2) the ~500 000 km^2 Sr isoscape of inland southeastern Australia recently published by our team (de Caritat et al., 2022b). The present study affords an opportunity to further redress this deficiency and will reduce the northern-hemisphere bias in future global $^{87}Sr/^{86}Sr$ models. It also pertains to a land surface that has not been rejuvenated by recent glaciation, consisting of over

80 85 % regolith or weathered material (Wilford, 2012), and as a result is abundant in minerals such as kaolinite, illite-smectite, goethite and hematite. The choice of total rather than bioavailable Sr as the focus of this work was driven by an emphasis on geological sources and processes.

2 Setting

The study area in northern Australia stretches across Western Australia, the Northern Territory and Queensland (hereafter

85 abbreviated to WA, NT and Qld, respectively) north of 21.5 °S (Figure 1). It is surrounded by the Indian Ocean to the west, the Timor and Arafura Seas and Gulf of Carpentaria to the north, and the Coral Sea (Pacific Ocean) to the east. The main climate zones in the area are described as 'Hot humid summer' in the north and along the coast, and 'Warm humid summer' further south and inland (BOM, 2022a). The vegetation zones are dominated by 'Tropical savanna' and 'Hot grassland with winter drought' (BOM, 2022b). The 10-year (1996-2005) average minimum and maximum temperatures mostly range 15-24

90 °C and 27-36 °C, respectively (BOM, 2022c). Average annual rainfall over the four-year period to November 2009 (when the bulk of the sampling was completed) mostly ranges 400-1500 mm/yr and is strongly seasonal (summer rain) (BOM, 2022d). Physiographically the study area includes, from west to east, the Kimberley, North Australian Plateaus, Barkly-Tanami Plains, Carpentaria Fall, Carpentaria Lowlands, Peninsular Uplands, and Burdekin Uplands Provinces (Pain et al., 2011). Topographic altitude ranges from sea level to 1622 m above sea level (asl) at Mt Bartle Frere (Qld's highest point,

95 located just south of Cairns), and the mean altitude is ~260 m asl (GA, 2008).

The soil types encountered in the study area are, according to the Australian Soil Classification scheme (Isbell et al., 2021; ASRIS, 2022a), most commonly vertosol, kandosol or tenosol (~24 % of the sample sites each), followed by rudosol, hydrosol or sodosol (7-9 %), and the rarer calcarosol, chromosol, dermosol or podosol (< 2 %). The major river basins that divide the area belong, from west to east, to the Pilbara, Sandy Desert-Mackay, Fitzroy, North Kimberley, Ord, Victoria, Tennant, Daly, Darwin, Melville, Alligator, Roper, Arnhem, McArthur, Channel Country, Burketown, Leichhardt, Flinders, Gilbert, Weipa, Mitchell, Princess Charlotte Bay, Burdekin, Barron, Cooper Creek, and Whitsunday Water Regions (GA, 1997). Landuse over the area is overwhelmingly 'Grazing natural vegetation', followed by 'Other protected areas (inc. indigenous uses)', then 'Nature conservation' (ASRIS, 2022b).
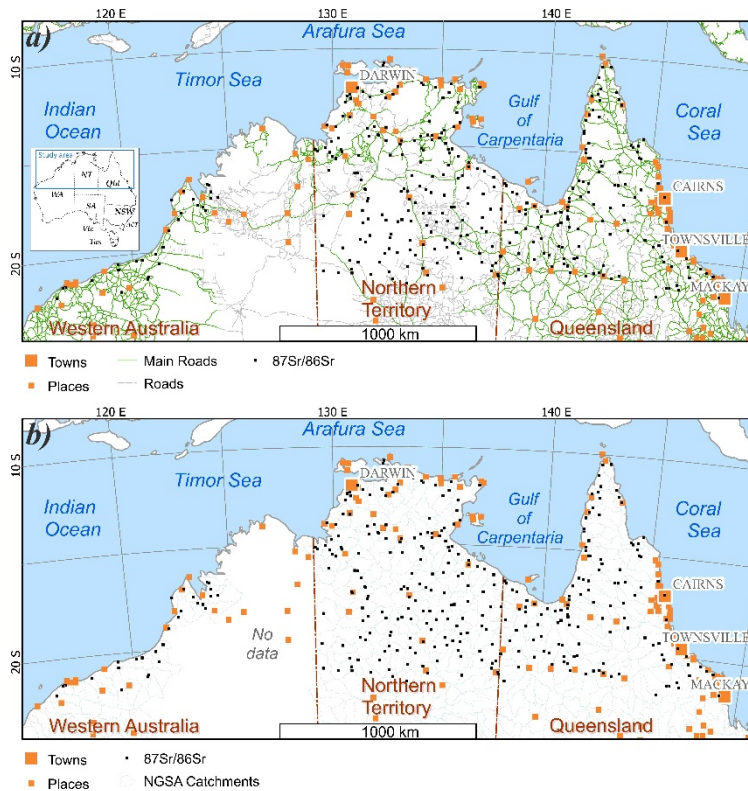
Figure 1. The northern Australia Sr isotope study area (see inset for location: WA – Western Australia, NT – Northern Territory, Qld – Queensland, NSW – New South Wales, ACT – Australian Capital Territory, Vic – Victoria, Tas – Tasmania, and SA – South Australia) and National Geochemical Survey of Australia (NGSA) and Northern Australia Geochemical Survey (NAGS) ^{87}Sr/^{86}Sr sample locations (small black squares) shown with towns (large grey squares) and places (medium grey squares) as well as (a) main roads (green solid lines), (secondary) roads (grey dashed lines); and (b) NGSA catchment boundaries (medium blue). Map projection: Albers equal area.

The main geological region groups (Blake and Kilgour, 1998) over the study area are, from west to east, the Pilbara, Canning, Kimberley, Bonaparte, Ord, Victoria River, Pine Creek, Victoria, Wiso, Arunta, Tennant, Money, McArthur, Arafura, Georgina, Isa, Carpentaria, Eromanga, Georgetown-Coen, Quinkan, and Paleozoic-Qld groups (see Supplement). The higher-level geological region domains (Blake and Kilgour, 1998) over the study area are, from west to east, the Pilbara,

4

Paleozoic, North-Australian Craton, Proterozoic, and Meso-Cenozoic domains (see Supplement). Thus, the study area displays a complex and protracted geological history spanning over 3.6 Gy (Ollier, 1988; Braun et al., 1998; Betts et al., 2002; Blewett, 2012; Withnall et al., 2013; Ahmad and Scrimgeour, 2013), with two cratonic nuclei in the west and centre (the Archean Pilbara Craton and Paleo- to Mesoproterozoic North-Australian Craton) flanked by younger Proterozoic and Paleozoic orogenic belts and basins, including the Phanerozoic Tasmanides to the east. Mesozoic and Cenozoic sedimentary sequences of the Eromanga and Carpentaria basins conceal much of the basement terrain over the eastern third of the study area. The whole region has experienced extensive weathering resulting in a ubiquitous and locally thick regolith mantle.

Figure 2a shows that by far the dominant bedrock unit intersected by the sample sites is 'Sedimentary and low-grade metamorphics' (89 % of sites), followed by the much less frequent 'Felsic igneous intrusive' (4 %), and 'Mafic to ultramafic igneous volcanic' (3 %) lithologies. Representing 2 % or less each are the lithologies 'Medium-grade metamorphics', 'Felsic to mafic igneous volcanic', 'High-grade metamorphics', 'Mafic igneous intrusive', and 'Felsic to intermediate igneous volcanic'. Investigating further the dominant bedrock unit 'Sedimentary and low-grade metamorphics' reveals that it is comprised of 'Regolith' (79 %), 'Sedimentary siliciclastic' (4 %), 'Feldspar- or lithic-rich arenite to rudite' (2 %), 'Sedimentary carbonate' (2 %), and < 1 % each of 'Argillaceous detrital sediment', 'Metasedimentary siliciclastic', and 'Quartz-rich arenite to rudite'. Further, the 'Regolith' class is reported to consist mainly 'Alluvium' (51 %), 'Sand plain' (9 %), 'Estuarine and delta deposit' (4 %), 'Colluvium' (4 %), 'Calcrete' (3 %), 'Undifferentiated sediment' (3 %), 'Lake deposit' (2 %), and < 2 % each of 'Black soil plain', 'Dune', and 'Ferruginous duricrust'.

The bedrock ages (periods) intersected at the sample sites are overwhelmingly Tertiary-Quaternary (58 %), followed by much less frequent Mesoproterozoic (8 %), and Cenozoic (6 %), Cambrian (5 %), Paleoproterozoic (5 %), Paleoproterozoic-Mesoproterozoic (3 %), Carboniferous-Permian (3 %), Permian (3 %), Devonian-Carboniferous (2 %), Archaean (2 %), and Cambrian-Ordovician (2 %). Representing < 2 % are the periods Devonian, Jurassic-Cretaceous, Ordovician, Silurian-Devonian, Jurassic, Neoproterozoic-Cambrian, and Triassic.

Numerous mineral occurrences are found in northern Australia and Figure 2b shows the most important ones classified as 'Mineral Deposits' (i.e. those with an inferred resource), 'Operating Mines' (currently producing), or 'Developing Projects' (approved but not yet producing). As mineralisation is the end-point of geologically 'unusual' processes taking place regionally in 'mineral systems' (Wyborn et al., 1994), it is useful to investigate if mineral system processes leave a recognisable $^{87}Sr/^{86}Sr$ fingerprint in the country rock and sediment derived therefrom. The study area is particularly well-endowed in 'Base Metal' deposits (both Pb-Zn- and Cu-dominated, e.g. Mount Isa, McArthur River, George Fisher) and is host to the 'North Australian Zinc Belt', the world's largest Zn-Pb province (Huston et al., 2022). In addition, notable occurrences of 'Battery or Alloy Metal' (Ni, Co, Mn, V, Mo, and Mg, e.g. Spinifex Ridge, Ripon Hills, Julia Creek, Richmond), and 'Precious Metal' (Au, Ag, e.g. Mount Isa, George Fisher) are also found here. Further, 'Other Metal' (Sn, Sb, W, Ta, Nb, e.g. Mount Carbine), 'Rare Earth Element' (e.g. Thunderbird, Nolans Bore), 'Platinum Group Element' (Pt, Pd, Rh, e.g. Munni Munni), and 'Heavy Mineral Sands' (Thunderbird) occurrences are also catalogued. Thus, the area is

significant for underpinning Australia's critical mineral resources supply now and into the future (e.g. DISER, 2022), without which a global transition to a lower-carbon economy will be challenging.
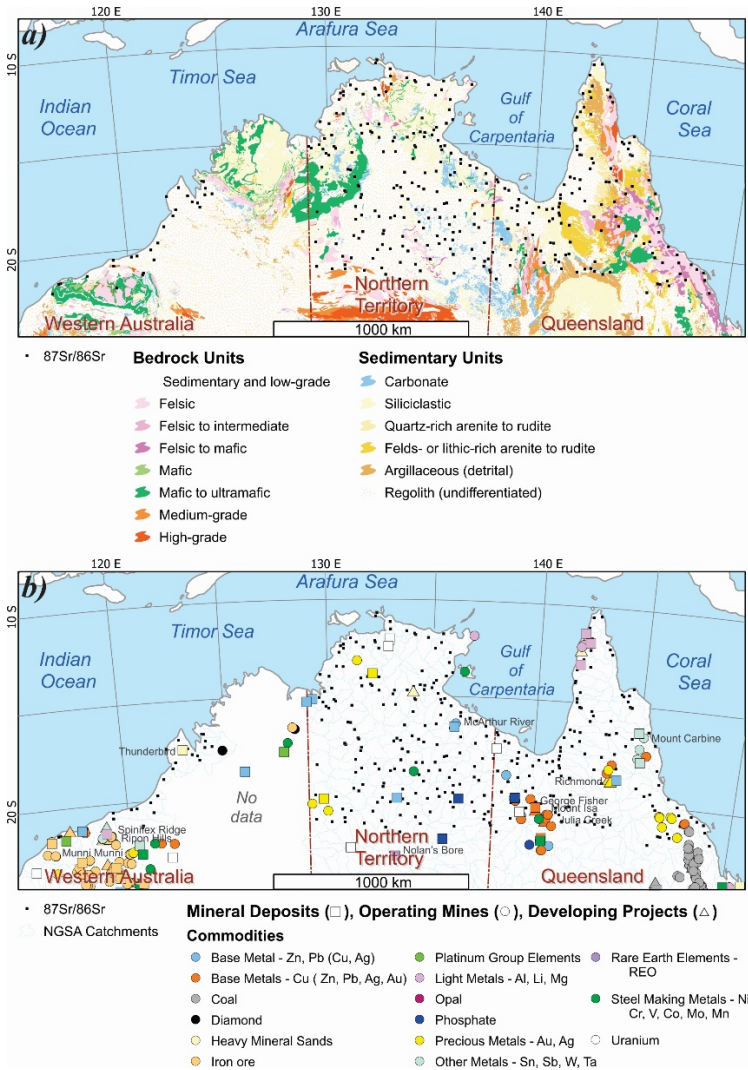
Figure 2. The northern Australia Sr isotope study area and National Geochemical Survey of Australia (NGSA) and Northern Australia Geochemical Survey (NAGS) ^{87}Sr/^{86}Sr sample locations (small black squares) shown with (a) surface geology from Raymond et al. (2012); and (b) NGSA catchment boundaries (medium blue) and mineral occurrences (GA, 2022a). Map projection: Albers equal area.

3 Material and methods

3.1 Material

This study makes use of archive 'catchment outlet sediment' samples collected during the National Geochemical Survey of Australia (NGSA), which covered ~80 % of Australia (de Caritat and Cooper, 2011a, 2016; de Caritat, 2022). The sampling

philosophy of the NGSA was to collect naturally mixed and fine-grained fluvial/alluvial sediments from large catchments,
160 thereby obtaining a representative average of the main soil and rock types contributing sediment through weathering. This
allowed an ultralow sampling density (~1 sample per 5200 km^2) still being representative of large-scale natural variations (de
Caritat and Cooper, 2011b). Catchment outlet sediments are similar to floodplain sediments in the sense that they are
deposited during receding floodwaters outside the riverbanks, but with the added complexity that, in Australia, many areas
can also experience addition (or loss) of aeolian material. The sampled floodplain geomorphological entities are typically
165 vegetated and biologically active (plants, worms, ants, etc.) thereby making the collected materials true soils, albeit soils
developed on transported alluvium parent material.

The sampling medium and density were both strategically chosen in the NGSA project to prioritize coverage over resolution.
This was justified by the fact that the NGSA was Australia's first and, to date, only fully integrated, internally consistent
geochemical survey with a truly national scope. In terms of the present study area, it is clear that these choices have
170 implications on the granularity of the patterns revealed by the Sr isoscape; as the collection of Sr isotope data in Australia
using NGSA samples grows in the future (e.g. de Caritat et al., 2022b, and this contribution), it is hoped the value of
coverage will prevail over a relative low resolution of detailed features.

The NGSA collected samples at two depths, a 'top outlet sediment' (TOS) from a shallow (0.1 m) soil pit approximately 0.8
m x 0.8 m in area, and a 'bottom outlet sediment' (BOS) from a minimum of three auger holes generally drilled within ~10
175 m of the TOS pit. The auger holes were drilled as deep as possible (to refusal or to maximum depth of 1 m), and the BOS
sample was collected on average from a depth of 0.6 m to 0.8 m from all augered holes. A field manual was compiled to
record all sample collection method details, including site selection (Lech et al., 2007). Sampling for the NGSA took place
between July 2007 and November 2009, and the field data were recorded in Cooper et al. (2010). In the laboratory, the
samples were air dried at 40 °C for a minimum of 48 h (or to constant mass) before being further prepared (see de Caritat et
180 al., 2009) for the comprehensive geochemical analysis program of the NGSA (see de Caritat et al., 2010). An aliquot of
minimum ~1 g of sample was milled to a fine powder using a carbon steel ring mill or, for a few samples only, an agate
micromill. The main sample type selected for the present Sr isotope study was NGSA BOS < 2 mm in order to be as
representative as possible of the geogenic background unaffected by modern landuse practices and inputs (e.g. fertilizers). A
few NGSA TOS < 2 mm samples, prepared in an identical fashion, were also analysed.
185 Several additional samples from the Northern Australia Geochemical Survey (NAGS; Bastrakov and Main, 2020) were
included in this project as they provide a higher density coverage over part of the study area. The NAGS project used the
same sampling philosophy and sample collection, preparation and analysis methods as the NGSA, with a higher sampling
density of 1 sample per ~500 km^2. The NAGS project collected only TOS (0-0.1 m depth) samples and the NAGS TOS < 2
mm aliquots were prepared and analysed as per the NGSA samples. Sampling for the NAGS took place in May and June
190 2017.

Overall 326 NGSA BOS < 2 mm, 18 NGSA TOS < 2 mm (including 15 with BOS also analysed), and 28 NAGS TOS
samples, for a total of 372 analyses from 357 samples, were analysed for Sr isotopes as detailed in the Methods Subsection

below. Given that there are ~10 % field duplicates in the NGSA and the smaller NAGS catchments are nested within NGSA catchments, all those samples originate from within 307 NGSA catchments, which together cover 1.536 million km^2 of northern Australia (see Figure 1).

3.2 Methods

Samples were prepared and analysed for Sr isotopes (^{87}Sr/^{86}Sr) at the Wollongong Isotope Geochronology Laboratory (WIGL). Approximately 50 mg of sample was weighed and digested in a 2:1 mixture of hydrofluoric and nitric acids. All reagents used were Seastar Baseline® grade, with Sr concentrations typically < 10 parts per trillion. Following digestion, samples were re-dissolved in aqua regia (twice if needed) in order to eliminate any fluorides, followed by nitric acid twice. Finally, samples were re-dissolved in 2 M nitric acid prior to ion exchange chromatography. Strontium was isolated from the sample matrix using automated, low-pressure chromatographic system Elemental Scientific prepFAST-MC™ and a 1 mL Sr–Ca column (Eichrom™) (Romaniello et al., 2015). The Sr elutions were re-dissolved in 0.3 M nitric acid. Strontium isotope analysis was performed on a Thermo Scientific Neptune Plus multicollector-inductively coupled plasma-mass spectrometer (MC-ICP-MS) at WIGL. The sample introduction system consists of an ESI Apex-ST PFA MicroFlow nebulizer with an uptake rate of ~0.1 mL min^{-1}, an SSI Quartz dual cyclonic spray chamber, jet sample, and X-skimmer cones. Measurements were performed in low-resolution mode. The instrument was tuned at the start of each session with a 20 parts per billion Sr solution, and sensitivity for ^{88}Sr was typically around 4 V. Masses 88, 87, 86, 85, 84, and 83 were collected on Faraday cups. Instrumental mass bias was internally corrected using measured ^{87}Sr/^{86}Sr. Masses 85 and 83 were used to correct for the isobaric interference of ^{87}Rb and ^{86}Kr, respectively. Maps were prepared using the open software QGis (version 3.16.14–Hannover) and applying an Albers equal area projection. Symbology for displaying ^{87}Sr/^{86}Sr data here was either point data classified in eight equal quantile classes (12.5 % of the data each; green = low to high = red) at the sampling site, or attributing this same value and colour to the whole catchment from which the outlet sediment comes, reflecting the sampling medium, catchment outlet sediment, being a representative sample of the average materials in the catchment (see Sect. 3.1).

3.3 Quality Assessment

National Institute of Standards and Technology (NIST) strontium carbonate isotope Standard Reference Material SRM987 was used as a secondary standard and measured after every five samples to assess accuracy during analysis. Accuracy of the whole procedure was assessed by processing United States Geological Survey (USGS) reference material Basalt from the Columbia River standard BCR-2 (Plumlee, 1998). The mean ± 2se ^{87}Sr/^{86}Sr for BCR-2 in this study is 0.704961 ± 35 (n = 13), within error of the value in Jweda et al. (2016) (0.704500 ± 11). Total procedure blanks ranged between 0.025 and 0.245 ng Sr (n = 12). Twenty field duplicate sample pairs (collected at a median distance of ~80 m from one another on the same landscape unit, see Lech et al., 2007) were analysed for ^{87}Sr/^{86}Sr in the BOS < 2 mm sample, and returned a median relative standard deviation of 0.17 %. The relative standard deviation from field duplicates includes natural variability

225   (mineralogical/chemical heterogeneity of the alluvial deposit), as well as sample collection, preparation, and analysis uncertainties.

Overall, we feel that the quality of the $^{87}Sr/^{86}Sr$ data presented herein is adequate for the purpose of regional mapping, and that reporting $^{87}Sr/^{86}Sr$ data to the third decimal place with an indicative fourth decimal place is appropriate for this work. This relatively low precision obtained for field duplicates is attributed to heterogeneity of the alluvial deposits, since

230   precision relating to sample preparation and analysis for Sr isotopes is at the fifth decimal place (see results for BCR-2 above).

3.4 Data Analysis

Data management was performed using Microsoft Excel®, graphing and visualization using IMDEX ioGas®, and spatial analysis and mapping using QGIS®, an open source geographical information system. For the purposes of generating the Sr

235   isoscape from combined BOS and TOS samples, calculated 'BOS-equivalent' values of TOS were derived from regression analysis (see Sect. 5.2). Catchment-based Sr isoscapes were constructed by assigning to each NGSA catchment the $^{87}Sr/^{86}Sr$ value of its outlet sediment sample, or, if more than one sample analysed per catchment (e.g. field duplicates or higher-resolution NAGS samples), the mean of those multiple samples. All maps are shown in Albers equal area projection.

4 Results

240   The soil $^{87}Sr/^{86}Sr$ values reported herein range from 0.7048 to 1.0330 (range = 0.3282). The median is 0.7405 and the mean 0.7532 (standard deviation = 0.0480; kurtosis = 8.1602; skewness = 2.4640). Figure 3 illustrates the univariate structure of the new data. Spatially, the $^{87}Sr/^{86}Sr$ values define large-scale, coherent patterns with multi-point low and high regions (Figure 4). The main high value (radiogenic) regions are found in the central and northern parts of the NT, most of Cape York, as well as along some of the coast including in the WA part of the study. Prominent low $^{87}Sr/^{86}Sr$ value (unradiogenic)

245   regions include a large, central, northwest-southeast trending elongated area in the NT, a smaller and similarly trending area in central Qld, as well as the northernmost and easternmost parts of the Qld study area.
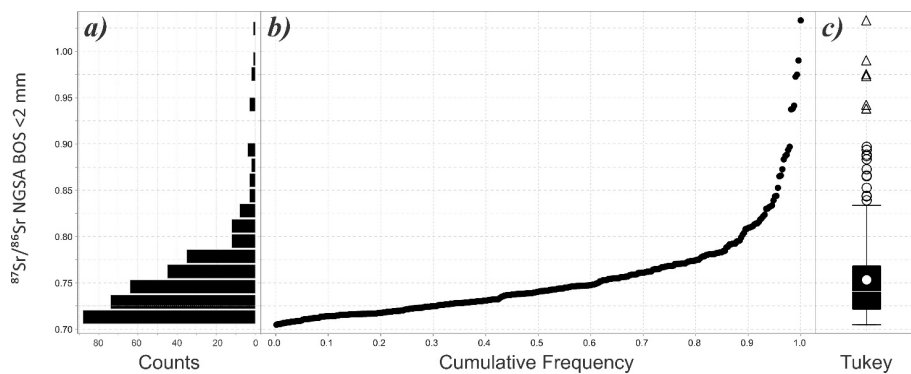
Figure 3. Univariate distribution of the ^{87}Sr/^{86}Sr data (n = 357) from the northern Australia Sr isotope study area: (a) histogram (20 bins 0.016 wide); (b) cumulative frequency plot; and (c) Tukey boxplot (mean = white dot; outliers = circles; and far outliers = triangles) (Tukey, 1977). Sample medium is the < 2 mm fraction of NGSA Bottom Outlet Sediment (BOS) or equivalent (see text for further information).
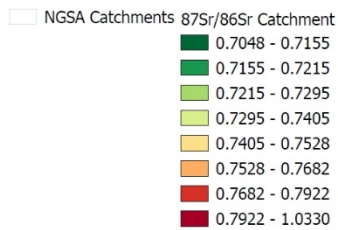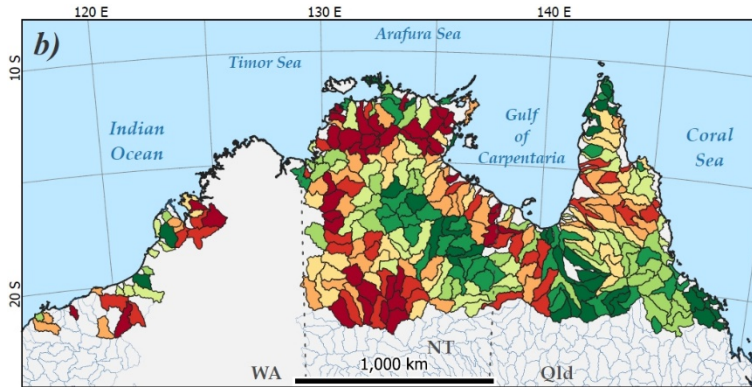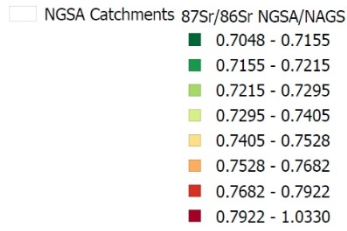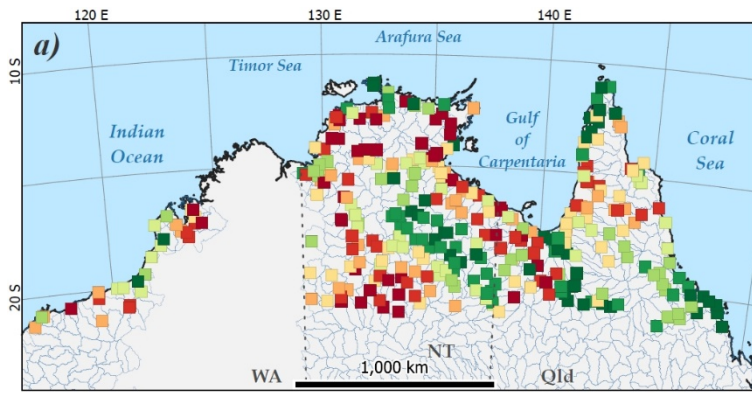
Figure 4. Strontium isoscape for the northern Australia study area with (a) data points classed by quantiles at the sampling sites; and (b) as whole catchments coloured by same colour ramp. Sample medium is the < 2 mm fraction of NGSA Bottom Outlet Sediment (BOS) or equivalent (see text for further information). Map projection: Albers equal area.

11

5 Discussion

260   **5.1 Comparison with other datasets**

A comparison of the present results with selected soil ^{87}Sr/^{86}Sr datasets from around the world is offered in Table 1. All discoverable data from Australia and the southern hemisphere comprising more than a handful of sites were included, whilst only selected northern hemisphere datasets focusing on recent and large-scale datasets were included. The table combines both bioavailable/exchangeable and bulk/total ^{87}Sr/^{86}Sr data, representing variable soil grain-size fractions (where reported),

265   parent materials and landuses. Despite that variability, one can make several observations. Firstly, the northern Australia Sr isotope dataset has the highest maximum (1.0330) and largest range (0.3282) of ^{87}Sr/^{86}Sr values amongst those compiled. Secondly, there is no observed standard protocol for collecting or preparing soils for either bioavailable or total ^{87}Sr/^{86}Sr determination. Thirdly, total ^{87}Sr/^{86}Sr datasets tend to have a wider range and greater variance than bioavailable ones, at least partly accounting for the higher values encountered here. These issues complicate data compilation and integration across

270   projects/countries, but do not preclude them. Indeed, through contemporaneous data analytics, including artificial intelligence and machine learning, it is likely that the relationships between bioavailable and total Sr isotope values and a host of other environmental variables (including from climatic, topographic, biotic and geoscientific categories) can be teased out and high-spatial resolution models/predictions of bioavailable or total Sr isotope distribution can be derived (e.g. Bataille et al., 2020). This is indeed a future research direction we propose/support for isoscape science in general, and an

275   Australian Sr isoscape in particular.

Table 1. Comparison of $^{87}Sr/^{86}Sr$ data from this study with selected datasets from around the world, with emphasis on Australia and the southern hemisphere (count, minimum, median, mean, standard deviation, maximum, and range). Regions = Aus: Australia; Qld: Queensland; SA: South Australia; SE: Southeastern; Vic: Victoria; WA: Western Australia. Digestions = AcAc: Acetic Acid (CH_3COOH); AmAc: Ammonium Acetate (CH_3COONH_4); AmNt: Ammonium Nitrate (NH_4NO_3); AR: Aqua Regia.

Region	Sample Type	Digestion	n	Min	Med	Mean	SD	Max	Range	Source
S Hemisphere: Australia										
Northern Aus	Soil (on alluvium), < 2 mm	Milled, HF + HNO_3 + AR	357	0.7048	0.7390	0.7527	0.0484	1.0330	0.3282	This study
SE Aus	Soil (on alluvium), < 2 mm	Milled, HF + HNO_3 + AR	112	0.7089	0.7199	0.7220	0.0736	0.7511	0.0422	de Caritat et al., 2022b
Mostly SA, Vic; 19 sites	Soil (calcrete)	AcAc	26	0.7061	0.7102	0.7115	0.0051	0.7329	0.0267	Quade et al., 1995
SE Aus; Murray Darling Basin	Alluvium, < 2 μm	HF + HNO_3	26	0.7080	0.7163	0.7267	0.0188	0.7751	0.0672	Gingele & De Deckker, 2005
Southern Aus; 8 sites	Soil (calcrete)	AcAc	46	0.7094	0.7151	0.7168	0.0058	0.7374	0.0280	Dart et al., 2007
	Soil (calcrete)	HNO_3 + HF + HCl	38	0.7125	0.7382	0.7538	0.0588	0.9985	0.2860	Dart et al., 2007
Canning Coast, WA	Dust, < 2 μm	AcAc	14	0.7141	0.7361	0.7385	0.0163	0.7727	0.0586	De Deckker, 2019
Cape York Peninsula, Qld	Soil, < 2 mm	AcAc	93	0.7075	0.7227	0.7252	0.0154	0.7911	0.0835	Adams et al., 2019
S Hemisphere: Other										
Brazil, 3 regions	Soil (agricultural), < 2 mm	AmAc	3	0.7122	0.7132	0.7129	0.0006	0.7133	0.0011	de Almeida, 2021
Southern Chile	Soil (forest)	AmAc	22	0.7091	0.7098	0.7101	0.0007	0.7119	0.0029	Kennedy et al., 2002
Southern Peru	Soil (agricultural)	Ashed, AmAc	114	0.7020	0.7076	0.7077	0.0017	0.7189	0.0169	Knudson et al., 2014
South Africa, 4 regions	Soil (agricultural), < 180 μm	HNO_3 + H_2O_2	67	0.7081	0.7130	0.7126	0.0020	0.7159	0.0078	Vorster at al., 2010
Southern New Zealand	Soil, < 2 mm	AmNt	83	0.7040	0.7079	0.7078	0.0013	0.7112	0.0072	A. Martin, pers. comm., 2021

Region	Sample Type	Digestion	n	Min	Med	Mean	SD	Max	Range	Source
N Hemisphere										
Britain	Soil	H_2O	26	0.7074	0.7093	0.7092	0.0010	0.7115	0.0041	Evans et al., 2010
France	Soil, < 2 mm	AmNt	524	0.7033	0.7113	0.7119	0.0042	0.7308	0.0275	Willmes et al., 2014
Europe	Soil (grazing), < 2 mm	AmNt	565	0.7038	0.7090	0.7103	0.0052	0.7523	0.0485	Hoogewerff et al., 2019
	Soil (agricultural), < 2 mm	AmNt	622	0.7038	0.7093	0.7112	0.0063	0.7596	0.0558	Hoogewerff et al., 2019
Israel	Soil, < 2 mm	AmNt	60	0.7058	0.7086	0.7085	0.0008	0.7102	0.0044	Moffat et al., 2020
Cambodia	Soil	Ashed, HF	60	0.7034	0.7115	0.7130	0.0060	0.7424	0.0389	Shewan et al., 2020
	Soil	Ashed, AmNt	46	0.7037	0.7110	0.7117	0.0039	0.7204	0.0167	Shewan et al., 2020
Japan	Soil, < 2 mm	H_2O_2	13	0.7067	0.7085	0.7088	0.0016	0.7129	0.0062	Oishi, 2021
Italy	Soil	Exchangeable and bulk	273	0.7053	0.7091	0.7099	0.0027	0.7238	0.0185	Lugli et al., 2022

5.2 Top-bottom relationship

285 Based on the 15 sites where both TOS and BOS samples were analysed, a strong correlation (Figure 5) between those two depths is found:

$$({}^{87}Sr/{}^{86}Sr)_{BOS} = 0.9913 \times ({}^{87}Sr/{}^{86}Sr)_{TOS} + 0.0069 \; (r^2 = 0.97; \; p < 0.001; \; n = 15). \tag{1}$$

Equation 1 was used to infer BOS ${}^{87}Sr/{}^{86}Sr$ from those sites where only TOS samples could be obtained (i.e. 3 NGSA and 28 NAGS sites), effectively deriving a 'BOS-equivalent' ${}^{87}Sr/{}^{86}Sr$ value for the purposes of performing internally consistent

290 statistical and spatial analysis.

As a result of the robust correlation between TOS and BOS, the BOS (or subsurface) Sr isoscapes of Figure 4 can be recalculated to TOS (or surface) Sr isoscapes by replacing the legend values for the eight quantile class boundaries by the values 0.7050 - 0.7156 - 0.7215 - 0.7293 - 0.7401 - 0.7522 - 0.7674 - 0.7910 - 1.0276. A TOS map and values would be useful when studying surface processes, such as plant and animal uptake or the effect of landuse on sediment composition
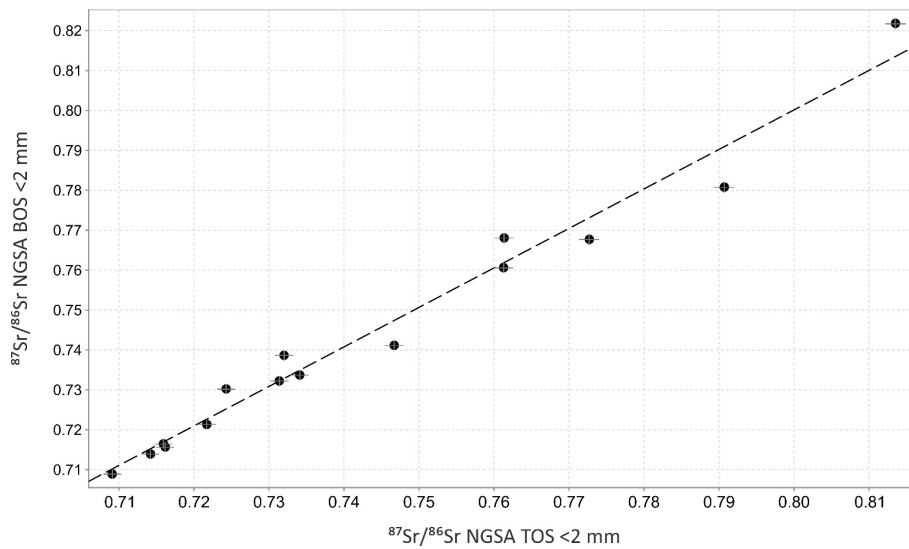
295 and dynamics.

Figure 5. Scatterplot of the BOS (deep) versus TOS (surface) $^{87}Sr/^{86}Sr$ data ($n = 15$) from the northern Australia Sr isotope study area with total uncertainty derived from field duplicates (0.17 %; grey plusses) and linear square regression line (dashed line).

5.3 Relationship to bedrock

300   When grouped by age of their respective geological region, the new $^{87}Sr/^{86}Sr$ data show a general trend of increasing $^{87}Sr/^{86}Sr$ with increasing bedrock age, as illustrated by the box and scatter plots of Figure 6. In this figure, average numerical ages (mid-points between beginning and end ages) are attributed to each geological period group. The observed trend is consistent with one of the known controls on mineral (and rock) $^{87}Sr/^{86}Sr$ values, namely their age.
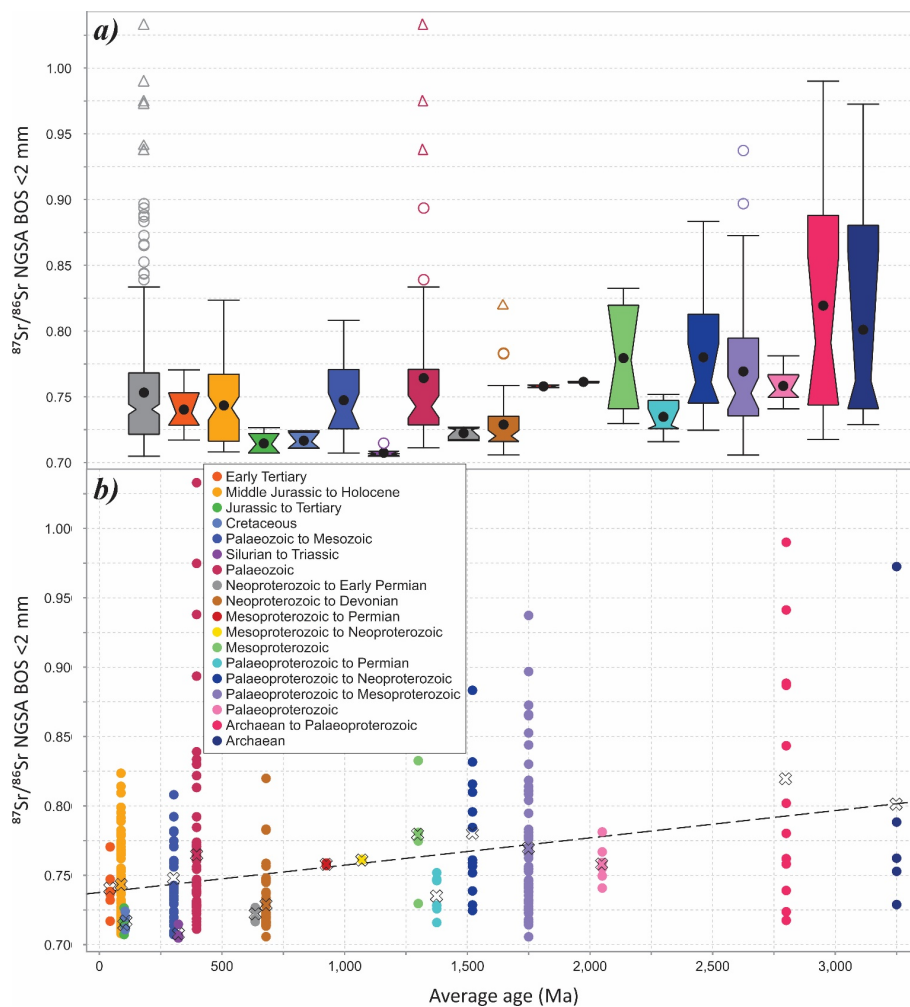
Figure 6. Distribution of the ^{87}Sr/^{86}Sr data from the northern Australia Sr isotope study area by geological region age: (a) notched Tukey boxplots (Tukey, 1977) of, left to right, the whole dataset first (grey; $n = 357$), then sorted by average age (Early Tertiary, $n = 6$; Middle Jurassic to Holocene, $n = 80$; Jurassic to Tertiary, $n = 5$; Cretaceous, $n = 4$; Palaeozoic to Mesozoic, $n = 28$; Silurian to Triassic, $n = 6$; Palaeozoic, $n = 61$; Neoproterozoic to Early Permian, $n = 7$; Neoproterozoic to Devonian, $n = 49$; Mesoproterozoic to Permian, $n = 2$; Mesoproterozoic to Neoproterozoic, $n = 2$; Mesoproterozoic, $n = 4$; Palaeoproterozoic to Permian, $n = 7$; Palaeoproterozoic to Neoproterozoic, $n = 13$; Palaeoproterozoic to Mesoproterozoic, $n = 59$; Palaeoproterozoic, $n = 7$; Archaean to Palaeoproterozoic, $n = 12$; and Archaean, $n = 5$); and (b) scatterplot against average age of the geological region with group averages (cross) and linear square regression line (dashed).

Another known control on Sr isotopic values is the Rb content, which over time contributes ^{87}Sr by radiogenic decay. Closer examination of the geology in the catchments with the 10 highest ^{87}Sr/^{86}Sr values indicates that they contain lithologies likely to be enriched in Rb relative to Sr (e.g. felsic, felsic-to-intermediate igneous rocks, medium- to high-grade metamorphic rocks) as shown by detailed maps in the Supplement. Of the five top-ten ^{87}Sr/^{86}Sr values in the northern NT, three are from the Pine Creek geological region. The two northernmost of these (samples #2007190099 and #2007191390) with ^{87}Sr/^{86}Sr = 0.9413 and 0.9900, respectively, are in catchments downstream of 1780-1790 Ma I-type granite intrusions

16

that have been reported to have $^{87}Sr/^{86}Sr$ from 0.71 to 8.13, $^{87}Rb/^{86}Sr$ = ~1 to 290, up to 956 mg/kg Rb and up to 459 mg/kg

320 Sr (Riley, 1980, table1).

The elevated samples from the WA coast are also generally proximal to, or downstream of, felsic igneous lithologies (including the granitoid and gneiss underlying the Mallina Basin; Van Kranendonk et al., 2002) and are consistent with $^{87}Sr/^{86}Sr$ values reported on clay fraction sediments from the region by De Deckker (2019) as shown in the Supplement. The northernmost samples along the coast of WA overlap with the King Leopold Orogen abutting the western flank of the

325 Kimberley geological region. Few $^{87}Sr/^{86}Sr$ data are available for this region, but those that exist within the Hooper Complex (Griffin et al., 2000) indicate radiogenic $^{87}Sr/^{86}Sr$ values: 0.7708-0.9620 for the Whitewater Volcanics, 0.7336-0.8524 for the Kongorow granite, and 0.7353-0.7602 for the Lennard granite (Bennett and Gellatly, 1970, table 2). Thus, observed elevated $^{87}Sr/^{86}Sr$ values of 0.8080, 0.7709, and 0.7923 in three sediment samples (#200719103, #2007190317, and #2007190966, respectively) near Derby, WA, are entirely compatible with these bedrock source rocks.

330 Page et al. (1980, table 5) published Rb and Sr data from the Alligator Rivers uranium field rocks, including from the Nimbuwah complex granitoid close to Cooper Creek, < 20 km north of the Nabarlek uranium deposit (their sample #7212.4063). For this sample they reported $^{87}Rb/^{86}Sr$ = 1.25-1.47, $^{87}Sr/^{86}Sr$ = 0.7387-0.7442, 146-164 mg/kg Rb and 320-336 mg/kg Sr. Our sample (#2007190710) from this same catchment has a $^{87}Sr/^{86}Sr$ value of 0.8019 and is located on a felsic granite polygon.

335 Black et al. (1983, tables 3 and 5) reported calculated initial rock $^{87}Sr/^{86}Sr$ ratios in the range 0.76 to 0.92 from granites, including the Wangala and the Haverson granites, in the northern Arunta geological region (southern NT). These intrusions intersect three sampled NGSA catchments for which we obtained elevated $^{87}Sr/^{86}Sr$ values, namely 0.8140, 0.7763, and 0.8651 (samples #2007190727, #2007190562, and #2007190123, respectively). These catchments are in turn just upstream of some of our top-ten $^{87}Sr/^{86}Sr$ values (between 0.8935 and 1.0330).

340 In the Georgetown geological region of northwestern Qld, broad consistency between whole rock $^{87}Sr/^{86}Sr$ and catchment sediment $^{87}Sr/^{86}Sr$ is also observed. For instance, our sample #2007190858, from a catchment that drains mostly the Esmeralda granite (average whole rock initial $^{87}Sr/^{86}Sr$ of 0.7314 ± 0.0116; Black, 1973, table 2) on the western edge of the Georgetown Inlier, has a relatively elevated $^{87}Sr/^{86}Sr$ value of 0.7467. Conversely, the three catchments that mostly directly drain the less radiogenic Newcastle Range Volcanics in the centre of the Inlier, which have a lower average whole rock

345 initial $^{87}Sr/^{86}Sr$ of 0.7152 ± 0.0011 (Black, 1973, table 2), have correspondingly lower sediment $^{87}Sr/^{86}Sr$ values of 0.7318 (#2007190572), 0.7268 (#2007190348), and a field duplicate pair of 0.7258 (#2007190548) and 0.7282 (#2007190548), respectively.

The floodplain sediment Sr isotopic values recorded in areas dominated by sedimentary carbonate and mafic/ultramafic igneous rocks are usually within an intermediate range between the more radiogenic and unradiogenic end-members

350 discussed above. Indeed, samples sited within 0.1 degree (~10 km) of lithologies recorded as sedimentary carbonate and mafic/ultramafic igneous rocks have median values of 0.7387 (n = 96) and 0.7422 (n = 42), respectively.

5.4 Relationship to mineralisation

Figure 7 illustrates the range of $^{87}Sr/^{86}Sr$ values of catchments that contain known mineralisation of various types. Forty four NGSA catchments host 97 mineral occurrences as catalogued by GA (2022a). These resources include 19 'Base Metal-Zn-Pb' – Zn, Pb (Cu, Ag); 17 'Battery/Alloy Metals' – Ni, Co, Mn, V, Mo, Mg; 13 'Precious Metals' – Au, Ag; 12 'Fertilizer Elements' – P, K; 6 'Rare Earth Elements'; 6 'Other Metals' – Sn, Sb, W, Ta, Nb; 5 'Iron Ore' – Fe; and 5 'Base Metal-Cu' – Cu (Zn, Pb, Ag, Au) occurrences. Whilst the vast majority of mineral occurrences are found in catchments with a sediment outlet $^{87}Sr/^{86}Sr$ signature << 0.84, six outlier occurrences are associated with higher catchment outlet sediment $^{87}Sr/^{86}Sr$ values: 0.8434 (Coronation Hill Pt, Pd deposit in the catchment containing sample #2007191552); 0.9373 (Nolans Bore hard rock REE and Mount Peake vanadium deposits the catchment containing sample #2007191112); 0.9748 (Batman Au deposit in the catchment containing sample #2007191329); and highest of all 0.9900 (Browns Pb-Zn and the Browns Co deposits in the catchment containing sample #2007191387). Some mineral occurrence types are not found in catchments with $^{87}Sr/^{86}Sr$ signature less radiogenic than 0.75 in this study: the minima reported for commodity groups 'Platinum Group Elements' being 0.7529; 'Rare Earth Element'/'Heavy Mineral Sands' 0.7606; and 'Diamond' 0.7567. Whilst it is unlikely that mineral deposits themselves impart a significant control on the $^{87}Sr/^{86}Sr$ of sediment collected down-catchment given their usually limited size, the hosting country rock, however, may potentially be more widely affected by mineral system processes, and appears to record some Sr isotopic effect that may be useful for mineral vectoring upon further investigation. One of the most radiogenic $^{87}Sr/^{86}Sr$ signatures (0.9373) is found for the catchment hosting both the Mount Peake V deposit (Simandl and Paradis, 2022) and the Nolans Bore hydrothermal REEs deposit (Schoneveld et al., 2015). Hydrothermal or magmatic REEs deposits are not usually characterised by highly radiogenic Sr signatures (e.g. 0.7029-0.7262 at Bayan Obo, Le Bas et al., 1997; 0.701-0.708 in global review of carbonatite deposits, Bolonin, 2019; 0.7037-0.7062 at Caotan, Wei et al., 2020) and nor does Nolans Bore specifically (0.7054 to 0.7079; Huston et al., 2016). Thus, the elevated $^{87}Sr/^{86}Sr$ reported here from this catchment is attributed to the radiogenic bedrock occurring in the study area and perhaps in upstream catchments immediately to the south of it.

18
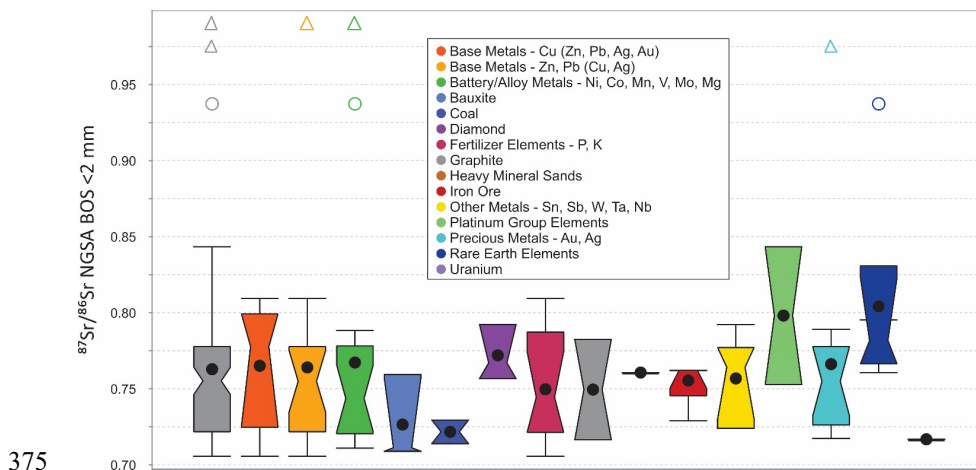
Figure 7. Distribution of the ^{87}Sr/^{86}Sr data from the northern Australia Sr isotope study area by mineral occurrence hosted in same catchment. From left to right, All (*n* = 97); 'Base Metals – Cu (Zn, Pb, Ag, Au)' (5); 'Base Metals – Zn, Pb (Cu, Ag)' (19); 'Battery/Alloy Metals – Ni, Co, Mn, V, Mo, Mg' (17); 'Bauxite' (3); 'Coal' (2); 'Diamond' (3); 'Fertilizer Elements – P, K' (12); 'Graphite' (2); 'Heavy Mineral Sands' (1); 'Iron Ore' (5); 'Other Metals – Sn, Sb, W, Ta, Nb' (6); P'latinum Group Elements' (2); 'Precious Metals – Au, Ag' (13); 'Rare Earth Elements' (6); and 'Uranium' (1).

6 Data availability

The new spatial Sr isotope dataset for the northern Australia region is publicly available from https://dx.doi.org/10.26186/147473 (de Caritat et al., 2022a) and through the Geoscience Australia portal https://portal.ga.gov.au/restore/cd686f2d-c87b-41b8-8c4b-ca8af531ae7e (last access: 27 February 2023). Metadata are also available through the Geoscience Australia portal (https://portal.ga.gov.au/metadata/geochronology-and-isotopes/isotopes/rbsr-isotope-points/4cacd9e8-3340-4c27-99fe-48d404e67ca8, last access 27 February 2023) (GA, 2022b).

7 Conclusions

Three hundred and seventy two new strontium (Sr) isotopic compositions (^{87}Sr/^{86}Sr) are reported from 357 catchment outlet sediment samples from northern Australia (north of 21.5 °S). The analysed material originates from the sample archives of the National Geochemical Survey of Australia (NGSA; *n* = 344) and Northern Australia Geochemical Survey (NAGS; 28) projects, both of which targeted overbank or floodplain landforms near the outlet of large catchments. The sampled catchments together cover 1.536 million km^2 of northern Australia. For the most part, bottom outlet sediment (BOS) samples, retrieved mostly by augering to, on average, 0.6 to 0.8m depth, were analysed. A few top outlet sediment (TOS) samples, collected from the top 0.1 m of soil, however, were also included, notably all the NAGS samples and 18 NGSA samples. *Total* digestion of milled < 2 mm grain-size fractions from these sediments yielded a wide range of ^{87}Sr/^{86}Sr values from a minimum of 0. 7048 to a maximum of 1.0330.

The present study represents the largest Sr isoscape in the southern hemisphere to-date, a region that is critically under-represented in terms of isotopic data worldwide. We found a very strong correlation between the ^{87}Sr/^{86}Sr values in the BOS and TOS samples, allowing us to confidently infer 'BOS-equivalent' values where only TOS samples were analysed. A map of the ^{87}Sr/^{86}Sr distribution (isoscape) across northern Australia reveals spatial patterns reflecting the ages and lithologies of the source material for the sediment, which is principally carried down catchment by fluvial processes. There is an overall increase in ^{87}Sr/^{86}Sr observed with increasing age of the geological region intersected at the sampling points. In areas of outcropping or subcropping felsic igneous rocks, relatively radiogenic Sr signatures are observed, and conversely for areas of mafic igneous rocks or marine sediments. The new Sr isotopic data are also interrogated in terms of the mineral occurrences found in their catchment. Whilst most mineral occurrences in the region are found in catchment with an ^{87}Sr/^{86}Sr signature << 0.84, six outlier occurrences are associated with higher values. Some mineral occurrence types ('Platinum Group Elements', 'Rare Earth Element'/'Heavy Mineral Sands', and 'Diamond') are not found in catchments with ^{87}Sr/^{86}Sr

signature less radiogenic than 0.75 in this study. Whether mineral system or regional petrogenetic processes are responsible for the association of relatively elevated $^{87}Sr/^{86}Sr$ with mineral deposits is a subject for further investigation.

410 Although we have focused the discussion of the new $^{87}Sr/^{86}Sr$ data on sediment sources in terms of rock ages and types, potential applications of the present isoscape and modelling derived therefrom could be extended to studies of mineralization, hydrology, food tracing, dust provenancing/sourcing, and historic migrations of people and animals.

425 **Publisher's note:** Copernicus Publications remains neutral with regard to jurisdictional claims in published maps and institutional affiliations.

References

Åberg, G., Jacks, G., and Hamilton, P. J.: Weathering rates and ^{87}Sr/^{86}Sr ratios: an isotopic approach, J. Hydrol., 109, 65–78, https://doi.org/10.1016/0022-1694(89)90007-3, 1989.

Åberg, G., Wickman, T., and Mutvei, H.: Strontium isotope ratios in mussel shells as indicators of acidification, Ambio, 24, 265–268, https://www.jstor.org/stable/4314345, 1995.

Åberg, G.: The use of natural strontium isotopes as tracers in environmental studies, Wat. Air Soil Poll., 79, 309–322, https://doi.org/10.1007/BF01100444, 1995.

Adams, S., Grün, R., McGahan, D., Zhao, J.-X., Feng, Y., Nguyen, A., Willmes, M., Quaresimin, M., Lobsey, B., Collard, M., and Westaway, M. C.: A strontium isoscape of north-east Australia for human provenance and repatriation, Geoarchaeol., 34, 231– 251, https://doi.org/10.1002/gea.21728, 2019.

Ahmad, M. and Scrimgeour, I. R.: Geological framework, Chap. 2 in: Geology and Mineral Resources of the Northern Territory, compiled by: Ahmad, M. and Munson, T. J., Northern Territory Geol. Surv., Special Publication, 5, 2:1–2:16, https://geoscience.nt.gov.au/gemis/ntgsjspui/bitstream/1/81482/1/GNT_Ch02_GeolFrame.pdf (last access: 27 February 2023), 2013.

Andersson, P. S., Wasserburg, G. J., and Ingri, J.: The sources and transport of Sr and Nd isotopes in the Baltic Sea, Earth Planet. Sci. Lett., 113, 459–472, https://doi.org/10.1016/0012-821X(92)90124-E, 1992.

Andersson, P. S., Wasserburg, G. J., Ingri, J., and Stordal, M. C. Strontium, dissolved and particulate loads in fresh and brackish waters: the Baltic Sea and Mississippi Delta, Earth Planet. Sci. Lett., 124, 195–210, https://doi.org/10.1016/0012-821X(94)00062-X, 1994.

Andersson, P., Lofvendahl, R., and Åberg, G.: Major element chemistry, δ^2H, δ^{18}O and ^{87}Sr/^{86}Sr in a snow profile across central Sweden, Atmos. Env., 24A, 2601–2608, https://doi.org/10.1016/0960-1686(90)90138-D, 1990.

Australian Soil Resource Information System (ASRIS): ASRIS Map Viewer Tool, Landcover Layer, Land Use 2001–2002, http://www.asris.csiro.au/mapping/viewer.htm (last access: 27 February 2023), 2022b.

Australian Soil Resource Information System (ASRIS): Digital Atlas of Australian Soils, ASRIS [data set], https://www.asris.csiro.au/themes/Atlas.html (last access: 27 February 2023), 2022a.

Bagheri, R., Nadri, A., Raeisi, E., Eggenkamp, H. G. M., Kazemi, G. A., and Montaseri, A.: Hydrochemical and isotopic (δ^{18}O, δ^2H, ^{87}Sr/^{86}Sr, δ^{37}Cl and δ^{81}Br) evidence for the origin of saline formation water in a gas reservoir, Chem. Geol., 384, 62–75, https://doi.org/10.1016/j.chemgeo.2014.06.017, 2014.

Bastrakov, E. N. and Main, P. T.: Northern Australia Geochemical Survey: a review of regional soil geochemical patterns, in: Exploring for the Future: Extended Abstracts, edited by: Czarnota, K., Roach, I., Abbott, S., Haynes, M., Kositcin, N., Ray, A., and Slatter, E., Geoscience Australia, Canberra, 1–4. http://dx.doi.org/10.11636/134367, 2020.

Bataille, C. P. and Bowen, G. J.: Mapping ^{87}Sr/^{86}Sr variations in bedrock and water for large scale provenance studies, Chem. Geol., 304, 39–52, https://doi.org/10.1016/j.chemgeo.2012.01.028, 2012.

Bataille, C. P., Brennan, S. R., Hartmann, J., Moosdorf, N., Wooller, M. J., and Bowen, G. J.: A geostatistical framework for predicting variability in strontium concentrations and isotope ratios in Alaskan rivers, Chem. Geol., 389, 1–15, https://doi.org/10.1016/j.chemgeo.2014.08.030, 2014.

Bataille, C. P., Crowley, B. E., Wooller, M. J., and Bowen, G. J.: Advances in global bioavailable strontium isoscapes, Palaeogeogr. Palaeocl. Palaeoecol., 555, 109849, https://doi.org/10.1016/j.palaeo.2020.109849, 2020.

Bataille, C. P., von Holstein, I. C. C., Laffoon, J. E., Willmes, M., Liu, X.- M., and Davies, G. R.: A bioavailable strontium isoscape for Western Europe: a machine learning approach, PLoS ONE, 13(5), e0197386, https://doi.org/10.1371/journal.pone.0197386, 2018.

Bathgate, H., Lovett, A., Clarke, J., Ueckermann, H., and Hoogewerff, J.: The use of $^{87}Sr/^{86}Sr$ ratios, trace elements and biological profiling for forensic provenancing of soils, Eur. Geoph. Union Gen. Assembly 2011, Geoph. Res. Abs., 13, EGU2011-6592, 2011.

505 Bennett, R. and Gellatly, D. C.: Rb-Sr age determinations of some rocks from the West Kimberley Region, Western Australia, Bur. Min. Res. Geol. Geoph. Record, 1970/20, 14 p, https://d28rz98at9flks.cloudfront.net/12433/Rec1970_020.pdf (last access: 27 February 2023), 1970.

Betts, P. G., Giles, D., Lister, G. S., and Frick, L. R.: Evolution of the Australian lithosphere, Austral. J. Earth Sci., 49, 661–695, https://doi.org/10.1046/j.1440-0952.2002.00948.x, 2002.

510 Black, L. P., Shaw, R. D., and Stewart, A. J.: Rb-Sr geochronology of Proterozoic events in the Arunta inlier, central Australia, Bur. Min. Res. J. Austral. Geol. Geoph., 8, 129–137, file://prod.lan/active/ops/cds/journals/Jou1983_v8_n2_p129/Jou1983_v8_n2_p129.pdf (last access: 27 February 2023), 1983.

Black, L. P.: Tables of Isotopic Ages from the Georgetown Inlier, North Queensland, Bur. Min. Res. Geol. Geoph. Record,

515 1973/50, 2 p, http://pid.geoscience.gov.au/dataset/ga/12874 (last access: 27 February 2023), 1973.

Blake, D. H. and Kilgour, B.: Geological Regions of Australia 1 : 5000 000 scale, Geosci. Austral., Canberra [data set], http://pid.geoscience.gov.au/dataset/ga/32366 (last access: 27 February 2023), 1998.

Blewett, R., editor: Shaping a Nation – A Geology of Australia, Geosci. Austral. and ANU E Press, Canberra, http://doi.org/10.22459/SN.08.2012, 2012.

520 Blum, J. D. and Erel, Y.: A silicate weathering mechanism linking increases in marine $^{87}Sr/^{86}Sr$ with global glaciation, Nature, 373, 415–418, https://doi.org/10.1038/373415a0, 1995.

Blum, J. D., Erel, Y., and Brown, K.: $^{87}Sr/^{86}Sr$ ratios of Sierra Nevada stream waters: implications for relative mineral weathering rates, Geochim. Cosmochim. Ac., 57, 5019–5025, https://doi.org/10.1016/S0016-7037(05)80014-6, 1994.

Bolonin, A.: Oxygen and carbon isotope composition in primary carbonatites of the world: data summary and linear trends.

525 Open J. Geol., 9, 424–439, https://doi.org/10.4236/ojg.2019.98028, 2019.

Braun, J., Dooley, J., Goleby, B., van der Hilst, R., and Klootwijk, C., editors: Structure and Evolution of the Australian Plate, Am. Geoph. Union, Geodyn. Series, 26, https://doi.org/10.1029/GD026, 1998.

Bullen, T. D., Blum, A. E., White, A. F., and Schulz, M. S.: A model for the temporal evolution of $^{87}Sr/^{86}Sr$ of the cation exchange pool in a simple granitoid weathering system: approach and implications, Eos, 75, 280–281, 1994.

530 Bullen, T., White, A., Blum, A., Harden, J., and Schulz, M.: Chemical weathering of a soil chronosequence on granitoid alluvium: II. Mineralogic and isotopic constraints on the behavior of strontium, Geochim. Cosmochim. Ac., 61, 291–306, https://doi.org/10.1016/S0016-7037(96)00344-4, 1997.

Bureau of Meteorology (BOM): Climate classification maps, http://www.bom.gov.au/jsp/ncc/climate_averages/climate-classifications/index.jsp?maptype=tmp_zones#maps (last access: 27 February 2023), 2022a.

535 Bureau of Meteorology (BOM): Decadal and multi-decadal temperature, http://www.bom.gov.au/jsp/ncc/climate_averages/decadal-temperature/index.jsp?maptype=1&period=9605 (last access: 27 February 2023), 2022c.

Bureau of Meteorology (BOM): Map of Climate Zones of Australia, http://www.bom.gov.au/climate/how/newproducts/images/zones.shtml (last access: 27 February 2023), 2022b.

540 Bureau of Meteorology (BOM): Recent and historical rainfall maps, http://www.bom.gov.au/climate/maps/rainfall/?variable=rainfall&map=totals&period=48month&region=nat&year=2009&month=11&day=30 (last access: 27 February 2023), 2022d.

Cartwright, I., Weaver, T., and Petrides, B.: Controls on $^{87}Sr/^{86}Sr$ ratios of groundwater in silicate-dominated aquifers: SE Murray Basin, Australia, Chem. Geol., 246, 107–123, https://doi.org/10.1016/j.chemgeo.2007.09.006, 2007.

545 Chadwick, O. A., Derry, L. A., Bern, C. R., and Vitousek, P. M.: Changing sources of strontium to soils and ecosystems across the Hawaiian Islands, Chem. Geol., 267, 64–76, https://doi.org/10.1016/j.chemgeo.2009.01.009, 2009.

Christensen, J. N., Dafflon, B., Shiel, A. E., Tokunaga, T. K., Wan, J., Faybishenko, B., Dong, W., Williams, K. H., Hobson, C., Brown, S. T., and Hubbard, S. S.: Using strontium isotopes to evaluate the spatial variation of groundwater recharge, Sci. Total Env., 637–638, 672–685, https://doi.org/10.1016/j.scitotenv.2018.05.019, 2018.

550 Collerson, K. D., Ullman, W. J., and Torgersen, T. Ground waters with unradiogenic $^{87}Sr/^{86}Sr$ ratios in the Great Artesian Basin, Australia, Geology, 16, 59–63, https://doi.org/10.1130/0091-7613(1988)016%3C0059:GWWUSS%3E2.3.CO;2, 1988.

Cooper, M., de Caritat, P., Burton, G., Fidler, R., Green, G., House, E., Strickland, C., Tang, J., and Wygralak, A.: National Geochemical Survey of Australia: Field Data, Record, 2010/18, Geosci. Austral., Canberra, 555 https://doi.org/10.11636/Record.2011.020, 2010.

Daneshvar, N., Azizi, H., Asahara, Y., Tsuboi, M., and Hosseini, M.: Rare earth elements and Sr isotope ratios of large apatite crystals in Ghareh Bagh mica mine, NW Iran: tracing for petrogenesis and mineralization, Minerals, 10, 833, https://doi.org/10.3390/min10090833, 2020.

Dart, R. C., Barovich, K. M., Chittleborough, D. J., and Hill, S. M.: Calcium in regolith carbonates of central and southern 560 Australia: its source and implications for the global carbon cycle, Palaeogeogr. Palaeocl. Palaeoecol., 249, 322–334, https://doi.org/10.1016/j.palaeo.2007.02.005, 2007.

de Almeida, B. S.: $^{87}Sr/^{86}Sr$ Isotopic Characterization as a Tool for the Designation of Origin and Geographical Indication: Application to Volcanic Rocks, Soils, Grapes and Wines from Brazil and Italy, Doctoral Thesis, University Frederic II of Naples, 106 pp, https://doi.org/10.13140/RG.2.2.15861.70882, 2021.

565 de Caritat, P. and Cooper, M.: A continental-scale geochemical atlas for resource exploration and environmental management: the National Geochemical Survey of Australia, Geochem. Explo. Env. Anal., 16, 3–13, https://doi.org/10.1144/geochem2014-322, 2016.

de Caritat, P. and Cooper, M.: National Geochemical Survey of Australia: Data Quality Assessment, Record, 2011/21, Geosci. Austral., Canberra, http://pid.geoscience.gov.au/dataset/ga/71971 (last access: 27 February 2023), 2011b.

570   de Caritat, P. and Cooper, M.: National Geochemical Survey of Australia: The Geochemical Atlas of Australia, Record, 2011/20, Geosci. Austral., Canberra, http://dx.doi.org/10.11636/Record.2011.020, 2011a.

de Caritat, P., Cooper, M., Lech, M., McPherson, A., and Thun, C.: National Geochemical Survey of Australia: Sample Preparation Manual, Record, 2009/08, Geosci. Austral., Canberra, http://pid.geoscience.gov.au/dataset/ga/68657 (last access: 27 February 2023), 2009.

575   de Caritat, P., Cooper, M., Pappas, W., Thun, C., and Webber, E.: National Geochemical Survey of Australia: Analytical Methods Manual, Record, 2010/15, Geosci. Austral., Canberra, http://pid.geoscience.gov.au/dataset/ga/70369 (last access: 27 February 2023), 2010.

de Caritat, P., Dosseto, A., and Dux, F.: A strontium isoscape of inland southeastern Australia. Earth Syst. Sci. Data, 14, 4271–4286. https://doi.org/10.5194/essd-14-4271-2022, 2022b

580   de Caritat, P., Dosseto, A., and Dux, F.: A strontium isoscape of northern Australia, Geosci. Austral., Canberra [data set], https://dx.doi.org/10.26186/147473, 2022a.

de Caritat, P., Kirste, D., Carr, G., and McCulloch, M.: Groundwater in the Broken Hill region, Australia: recognising interaction with bedrock and mineralisation using S, Sr and Pb isotopes, Appl. Geochem., 20, 767–787, https://doi.org/10.1016/j.apgeochem.2004.11.003, 2005.

585   de Caritat, P.: The National Geochemical Survey of Australia: review and impact. Geochemistry: Exploration, Environment, Analysis, geochem2022-032, https://doi.org/10.1144/geochem2022-032, 2022.

De Deckker, P., Munday, C. I., Brocks, J., O'loingsigh, T., Allison, G. E., Hope, J., Norman, M., Stuut, J.- B. W., Tapper, N. J., and van der Kaars, S.: Characterisation of the major dust storm that traversed over eastern Australia in September 2009; a multidisciplinary approach, Aeol. Res., 15, 133–149, https://doi.org/10.1016/j.aeolia.2014.07.003, 2014.

590   De Deckker, P.: Airborne dust traffic from Australia in modern and Late Quaternary times, Global Planet. Change, 184, 103056, https://doi.org/10.1016/j.gloplacha.2019.103056, 2020.

De Deckker, P.: OZ-3 northern Western Australia sampling trip and analysis: strontium, rubidium and neodymium isotopes, Pangaea, https://doi.pangaea.de/10.1594/PANGAEA.907689, 2019.

Denison, R. E., Koepnick, R. B., Burke, W. H., Hetherington, E. A., and Fletcher, A.: Construction of the Mississippian,
595   Pennsylvanian and Permian seawater ^{87}Sr/^{86}Sr curve, Chem. Geol., 112, 145–167, https://doi.org/10.1016/0009-2541(94)90111-2, 1994a.

Denison, R. E., Koepnick, R. B., Fletcher, A., Howell, M. W., and Callaway, W. S.: Criteria for the retention of original seawater ^{87}Sr/^{86}Sr in ancient shelf limestones, Chem. Geol., 112, 131–143, https://doi.org/10.1016/0009-2541(94)90110-4, 1994b.

600   Department of Industry, Science, Energy and Resources (DISER): 2022 Critical Minerals Strategy, Aust. Gov., Canberra, https://www.industry.gov.au/publications/critical-minerals-strategy-2022, last access: 27 February 2023, 2022.

Di Paola-Naranjo, R. D., Baroni, M. V., Podio, N. S., Rubinstein, H. R., Fabani, M. P., Badini, R. G., Inga, M., Ostera, H. A., Cagnoni, M., Gallegos, E., Gautier, E., Peral-Garcia, P., Hoogewerff, J., and Wunderlin, D. A.: Fingerprints for main varieties of Argentinean wines: terroir differentiation by inorganic, organic, and stable isotopic analyses coupled to chemometrics, J. Ag. Food Chem., 59, 7854–7865, https://doi.org/10.1021/jf2007419, 2011.

Dogramaci, S. S. and Herczeg, A. L.: Strontium and carbon isotope constraints on carbonate-solution interactions and inter-aquifer mixing in groundwaters of the semi-arid Murray Basin, Australia, J. Hydrol., 262, 50–67, https://doi.org/10.1016/S0022-1694(02)00021-5, 2002.

Douglas, G. B., Gray, C. M., Hart, B. T., and Beckett, R.: A strontium isotopic investigation of the origin of suspended particulate matter (SPM) in the Murray-Darling River system, Australia, Geochim. Cosmochim. Ac., 59, 3799–3815, https://doi.org/10.1016/0016-7037(95)00266-3, 1995.

Douglas, G. B., Gray, C. M., Hart, B. T., and Beckett, R.: A strontium isotopic investigation of the origin of suspended particulate matter (SPM) in the Murray-Darling River system, Australia, Geochim. Cosmochim. Ac., 59, 3799–3815, https://doi.org/10.1016/0016-7037(95)00266-3, 1995.

Evans, J. A., Montgomery, J., Wildman, G., and Boulton, N.: Spatial variations in biosphere ^{87}Sr/^{86}Sr in Britain, J. Geol. Soc., 167, 1–4, https://doi.org/10.1144/0016-76492009-090, 2010.

Faure, G. and Felder, R. P.: Isotopic composition of strontium and sulfur in secondary gypsum crystals, Brown Hills, Transantarctic Mountains, J. Geoch. Explo., 14, 265–270, https://doi.org/10.1016/0375-6742(81)90116-3, 1981.

Flecker, R., de Villiers, S., and Ellam, R.M.: Modelling the effect of evaporation on the salinity-^{87}Sr/^{86}Sr relationship in modern and ancient marginal-marine systems: the Mediterranean Messinian Salinity Crisis, Earth Planet. Sci. Lett., 203, 221–233, https://doi.org/10.1016/S0012-821X(02)00848-8, 2002.

Frei, R. and Frei, K. M.: The geographic distribution of Sr isotopes from surface waters and soil extracts over the island of Bornholm (Denmark) – A base for provenance studies in archeology and agriculture, Appl. Geochem., 38, 147–160, https://doi.org/10.1016/j.apgeochem.2013.09.007, 2013.

Geoscience Australia (GA): 9 Second Digital Elevation Model of Australia Version 3, Geosci. Austral., Canberra [data set], http://pid.geoscience.gov.au/dataset/ga/89580 (last access: 27 February 2023), 2008.

Geoscience Australia (GA): Australia's River Basins 1997 – Product User Guide, Geosci. Austral., Canberra, http://pid.geoscience.gov.au/dataset/ga/42343 (last access: 27 February 2023), 1997.

Geoscience Australia (GA): Australian Operating Mines Map 2021 Data, Geosci. Austral., Canberra [data set], https://dx.doi.org/10.26186/147010 (last access: 27 February 2023), 2022a.

Geoscience Australia: Geoscience Australia Portal: Geochronology and Isotopes – Isotopes – Rb-Sr Isotope – Points, Australian Government [data set], https://portal.ga.gov.au/metadata/geochronology-and-isotopes/isotopes/rbsr-isotope-points/4cacd9e8-3340-4c27-99fe-48d404e67ca8 (last access: 27 February 2023), 2022b.

Gingele, F. X. and De Deckker, P.: Clay mineral, geochemical and Sr-Nd-isotopic fingerprinting of sediments in the Murray-Darling fluvial system, southeast Australia, Aust. J. Earth Sci., 52, 965–974, https://doi.org/10.1080/08120090500302301, 2005.

Gosselin, D. C., Harvey, F. E., Frost, C., Stotler, R., and Macfarlane, P. A.: Strontium isotope geochemistry of groundwater in the central part of the Dakota (Great Plains) aquifer, USA, Appl. Geochem., 19, 359–377, https://doi.org/10.1016/S0883-2927(03)00132-X, 2004.

Gosz, J. R., Brookins, D.G., and Moore, D.I.: Using strontium isotope ratios to estimate inputs to ecosystems, Biosci., 33, 23–30, https://doi.org/10.2307/1309240, 1983.

Graustein, W. C.: $^{87}Sr/^{86}Sr$ ratios measure the sources and flow of strontium in terrestrial ecosystems, Chap. 28 in: Stable Isotopes in Ecological Research, edited by: Rundel, P. W., Ehleringer, J. R., and Nagy, K. A., Springer-Verlag, New York: 491–512, https://doi.org/10.1007/978-1-4612-3498-2_28, 1989.

Green, G. P., Bestland, E. A., and Walker, G. S.: Distinguishing sources of base cations in irrigated and natural soils: evidence from strontium isotopes, Biogeochem., 68, 199–225, https://doi.org/10.1023/B:BIOG.0000025743.34079.d3, 2004.

Griffin, T. J., Page, R., Sheppard, S., and Tyler, I.: Tectonic implications of Palaeoproterozoic post-collisional, high-K felsic igneous rocks from the Kimberley region of northwestern Australia, Precambrian Research, 101, 1–23. https://doi.org/10.1016/S0301-9268(99)00084-4, 2000.

Grobe, M., Machel, H. G., and Heuser, H.: Origin and evolution of saline groundwater in the Münsterland Cretaceous Basin, Germany: oxygen, hydrogen, and strontium isotope evidence, J. Geoch. Explo., 69–70, 5–9, https://doi.org/10.1016/S0375-6742(00)00009-1, 2000.

Gruszczynski, M., Hoffman, A., Krzysztof, M., and Veizer, J.: Seawater strontium isotopic perturbation at the Permian-Triassic boundary, west Spitsbergen, and its implications for the interpretation of strontium isotopic data, Geology, 20, 779–782, https://doi.org/10.1130/0091-7613(1992)020%3C0779:SSIPAT%3E2.3.CO;2, 1992.

Hagedorn, B., Cartwright, I., Raveggi, M., and Maas, R.: Rare earth element and strontium geochemistry of the Australian Victorian Alps drainage system: Evaluating the dominance of carbonate vs. aluminosilicate weathering under varying runoff, Chem. Geol., 284, 105–126, https://doi.org/10.1016/j.chemgeo.2011.02.013, 2011.

Harrington, G. A. and Herczeg, A. L.: The importance of silicate weathering of a sedimentary aquifer in arid Central Australia indicated by very high $^{87}Sr/^{86}Sr$ ratios, Chem. Geol., 199, 281–292, https://doi.org/10.1016/S0009-2541(03)00128-1, 2003.

Hoogewerff, J. A., Reimann, C., Ueckermann, H., Frei, R., Frei, K. M., van Aswegen, T., Stirling, C., Reid, M., Clayton, A., Ladenberger, A., and The GEMAS Project Team: Bioavailable $^{87}Sr/^{86}Sr$ in European soils: a baseline for provenancing studies, Sci. Total Environ., 672, 1033–1044, https://doi.org/10.1016/j.scitotenv.2019.03.387, 2019.

Huston, D. L., Champion, D. C., Czarnota, K., Duan, J., Hutchens, M., Paradis, S., Hoggard, M., Ware, B., Gibson, G. M., Doublier, M. P., Kelley, K., McCafferty, A., Hayward, N., Richards, F., Tessalina, S., and Carr, G.: Zinc on the edge–

isotopic and geophysical evidence that cratonic edges control world-class shale-hosted zinc-lead deposits. Miner. Deposita, https://doi.org/10.1007/s00126-022-01153-9, 2022.

670   Huston, D. L., Maas, R., Cross, A., Hussey, K. J., Mernagh, T. P., Fraser, G., and Champion, D. C.: The Nolans Bore rare-earth element-phosphorus-uranium mineral system: geology, origin and post-depositional modifications, Miner. Deposita, 51, 797–822, https://doi.org/10.1007/s00126-015-0631-y, 2016.

Isbell, R. F. and National Committee on Soil and Terrain: The Australian Soil Classification, third edn., CSIRO Publishing, Melbourne, Victoria, 181 pp., https://ebooks.publish.csiro.au/content/australian-soil-classification-9781486314782 (last access: 27 February 2023), 2021.

675   Jacks, G., Åberg, G., and Hamilton, P. J.: Calcium budgets for catchments as interpreted by strontium isotopes, Hydrol. Res., 20, 85–96, https://doi.org/10.2166/nh.1989.0007, 1989.

Jomori, Y., Minami, M., Sakurai-Goto, A., and Ohta, A.: Comparing the $^{87}Sr/^{86}Sr$ of the bulk and exchangeable fractions in stream sediments: implications for $^{87}Sr/^{86}Sr$ mapping in provenance studies, Appl. Geochem., 86, 70–83, https://doi.org/10.1016/j.apgeochem.2017.09.004, 2017.

680   Jweda, J., Bolge, L., Class, C., and Goldstein, S. L.: High precision Sr-Nd-Hf-Pb isotopic compositions of USGS reference material BCR-2, Geostand. Geoanal. Res., 40, 101–115, https://doi.org/10.1111/j.1751-908X.2015.00342.x, 2016.

Kennedy, M. J., Hedin, L. O., and Derry, L. A.: Decoupling of unpolluted temperate forests from rock nutrient sources revealed by natural $^{87}Sr/^{86}Sr$ and ^{84}Sr tracer addition, Proc. Nat. Acad. Sci., 99, 9639–9644, https://doi.org/10.1073/pnas.152045499, 2002.

685   Knudson, K. J., Webb, E., White, C., and Longstaffe, F. J.: Baseline data for Andean paleomobility research: a radiogenic strontium isotope study of modern Peruvian agricultural soils, Archaeol. Anthropol. Sci., 6, 205–219, https://doi.org/10.1007/s12520-013-0148-1, 2014.

Le Bas, M., Spiro, B., and Yang, X.: Oxygen, carbon and strontium isotope study of the carbonatitic dolomite host of the Bayan Obo Fe-Nb-REE deposit, Inner Mongolia, N China, Mineral. Mag., 61, 531–541, 690   https://doi.org/10.1180/minmag.1997.061.407.05, 1997.

Lech, M. E., de Caritat, P., and Mcpherson, A. A.: National Geochemical Survey of Australia: Field Manual, Record, 2007/08, Geosci. Austral., Canberra, http://pid.geoscience.gov.au/dataset/ga/65234 (last access: 27 February 2023), 2007.

Lugli, F., Cipriani, A., Bruno, L., Ronchetti, F., Cavazzuti, C., and Benazzi, S.: A strontium isoscape of Italy for provenance studies, Chem. Geol., 587, 120624, https://doi.org/10.1016/j.chemgeo.2021.120624, 2022.

695   Lyons, W. B., Tyler, S. W., Gaudette, H. E., and Long, D. T.: The use of strontium isotopes in determining groundwater mixing and brine fingering in a playa spring zone, Lake Tyrrell, Australia, J. Hydrol., 167, 225–239, https://doi.org/10.1016/0022-1694(94)02601-7, 1995.

McArthur, J. M., Howarth, R. J., and Shields, G. A.: Strontium Isotope Stratigraphy, Chap. 7 in: The Geologic Time Scale, edited by: F. M., Ogg, J. G., Schmitz, M., and Ogg, G., Elsevier BV, 127–144, https://doi.org/10.1016/B978-0-12-824360-700   2.00007-3, 2012.

McNutt R. H.: Strontium Isotopes. In: Environmental Tracers in Subsurface Hydrology, edited by: Cook P. G. and Herczeg A. L., Springer, Boston, MA, https://doi.org/10.1007/978-1-4615-4557-6_8, 2000.

McNutt, R. H., Frape, S. K., and Dollar, P.: A strontium, oxygen and hydrogen isotopic composition of brines, Michigan and Appalachian Basins, Ontario and Michigan, Appl. Geochem., 2, 495–505, https://doi.org/10.1016/0883-2927(87)90004-7, 1987.

Moffat, I., Rudd, R., Willmes, M., Mortimer, G., Kinsley, L., McMorrow, L., Armstrong, R., Aubert, M., and Grün, R.: Bioavailable soil and rock strontium isotope data from Israel. Earth Syst. Sci. Data, 12, 3641–3652, https://doi.org/10.5194/essd-12-3641-2020, 2020.

Mountjoy, E. W., Qing, H., and McNutt, R. H.: Strontium isotopic composition of Devonian dolomites, Western Canada Sedimentary Basin: significance of sources of dolomitizing fluids, Appl. Geochem., 7, 59–75, 1992.

Nebel O., Stammeier J. A.: Strontium Isotopes. In: Encycl. Geochem., Encycl. Earth Sci. Series, edited by: White W. M., Springer, Cham. https://doi.org/10.1007/978-3-319-39312-4_137, 2018.

Négrel, P. and Grosbois, C.: Changes in chemical and $^{87}Sr/^{86}Sr$ signature distribution patterns of suspended matter and bed sediments in the upper Loire river basin (France), Chem. Geol., 156, 231–249, https://doi.org/10.1016/S0009-2541(98)00182-X, 1999.

Négrel, P. and Pauwels, H.: Interaction between different groundwaters in Brittany catchments (France): characterizing multiple sources through strontium- and sulphur isotope tracing, Wat. Air Soil Poll., 151, 261–285, https://doi.org/10.1023/B:WATE.0000009912.04798.b7, 2004.

Oishi, Y.: Is the Sr isotope ratio of mosses a good indicator for Asian dust (Kosa)? Landscape Ecol. Eng., https://doi.org/10.1007/s11355-021-00476-5, 2021.

Ojiambo, S. B., Lyons, W. B., Welch, K. A., Poreda, R. J., and Johannesson, K. H.: Strontium isotopes and rare earth elements as tracers of groundwater-lake water interactions, Lake Naivasha, Kenya, Appl. Geochem., 18, 1789–1805, https://doi.org/10.1016/S0883-2927(03)00104-5, 2003.

Oliver, L., Harris, N., Bickle, M., Chapman, H., Dise, N., and Horstwood, M.: Silicate weathering rates decoupled from the $^{87}Sr/^{86}Sr$ ratio of the dissolved load during Himalayan erosion, Chem. Geol., 201, 119–139, https://doi.org/10.1016/S0009-2541(03)00236-5, 2003.

Ollier, C. D.: The regolith in Australia, Earth-Sci. Rev., 25, 355–361, https://doi.org/10.1016/0012-8252(88)90003-7, 1988.

Pacheco-Forés, S. I., Gordon, G. W., and Knudson, K. J.: Expanding radiogenic strontium isotope baseline data for central Mexican paleomobility studies, PLoS ONE, 15, e0229687, https://doi.org/10.1371/journal.pone.0229687, 2020.

Page, R. W., Needham, R. S., and Compston, W.: Geochronology and evolution of the Late-Archaean basement and Proterozoic rocks in the Alligator Rivers uranium field, Northern Territory, Australia, in: Proc. Int. Uranium Symp., Pine Creek Geosyncline (Sydney, New South Wales, 4-8 June 1979), edited by: Ferguson, J. and Goleby, A. B., Int. Atom. En. Agency, Vienna, Austria, 39–68, https://inis.iaea.org/collection/NCLCollectionStore/_Public/12/629/12629252.pdf, last access: 27 February 2023, 1980.

735 Pain, C., Gregory, L., Wilson, P., and McKenzie, N.: The Physiographic Regions of Australia – Explanatory Notes, Australian Collaborative Land Evaluation Program (ACLEP) and National Committee on Soil and Terrain (NCST), Canberra, 30 pp., https://publications.csiro.au/rpr/pub?pid=csiro%3AEP113843 (last access: 27 February 2023), 2011.

Palmer, M. R., Helvaci, C., and Fallick, A. E.: Sulphur, sulphate oxygen and strontium isotope composition of Cenozoic Turkish evaporates, Chem. Geol., 209, 341–356, https://doi.org/10.1016/j.chemgeo.2004.06.027, 2004.

740 Plumlee, G.: Basalt, Columbia River, BCR-2, Prelim. U.S. Geol. Surv. Cert. Anal., https://cpb-us-w2.wpmucdn.com/muse.union.edu/dist/c/690/files/2021/07/usgs-bcr2-1.pdf (last access: 27 February 2023), 1998.

Price, G. J., Ferguson, K. J., Webb, G. E., Feng, Y. X., Higgins, P., Nguyen, A. D., Zhao, J. X., Joannes-Boyau, R., and Louys, J.: Seasonal migration of marsupial megafauna in Pleistocene Sahul (Australia-New Guinea), P. Roy. Soc. B-Biol. Sci., 284, 20170785, https://doi.org/10.1098/rspb.2017.0785, 2017.

745 Probst, A., El Gh'Mari, A., Aubert, D., Fritz, B., and McNutt, R.: Strontium as a tracer of weathering processes in a silicate catchment polluted by acid atmospheric inputs, Strengbach, France, Chem. Geol., 170, 203–219, https://doi.org/10.1016/S0009-2541(99)00248-X, 2000.

Quade, J., Chivas, A. R., and McCulloch, M. T.: Strontium and carbon isotope tracers and the origins of soil carbonate in South Australia and Victoria, Palaeogeogr. Palaeocl. Palaeoecol., 113, 103–117, https://doi.org/10.1016/0031-750 0182(95)00065-T, 1995.

Raymond, O. L. (Ed.), Gallagher, R. (Ed.), Shaw, R., Yeates, A. N., Doutch, H. F., Palfreyman, W. D., Blake, D. H., and Highet, L.: Surface Geology of Australia 1 : 2.5 million scale dataset 2012 edition, Geosci. Austral., Canberra [data set], https://doi.org/10.26186/5c636e559cbe1, 2012.

Revel-Rolland, M., De Deckker, P., Delmonte, B., Hesse, P. P., Magee, J. W., Basile-Doelsch, I., Grousset, F., and Bosch, 755 D.: Eastern Australia: a possible source of dust in East Antarctica interglacial ice, Earth Planet. Sci. Lett., 249, 1–13, https://doi.org/10.1016/j.epsl.2006.06.028, 2006.

Riley, G. H.: Granite ages in the Pine Creek Geosyncline, in: Proc. Int. Uranium Symp., Pine Creek Geosyncline (Sydney, New South Wales, 4-8 June 1979), edited by: Ferguson, J. and Goleby, A. B., Int. Atom. En. Agency, Vienna, Austria, 69–72, https://inis.iaea.org/collection/NCLCollectionStore/_Public/12/629/12629252.pdf, last access: 27 February 2023, 1980.

760 Romaniello, S. J., Field, M. P., Smith, H. B., Gordon, G. W., Kim, M. H., and Anbar, A. D.: Fully automated chromatographic purification of Sr and Ca for isotopic analysis, J. Anal. Atomic Spectro., 30, 1906–1912, https://doi.org/10.1039/C5JA00205B, 2015.

Rotenberg, E., Davis, D. W., Amelin, Y., Ghosh, S., and Bergquist, B. A.: Determination of the decay-constant of ^{87}Rb by laboratory accumulation of ^{87}Sr, Geochim. Cosmochim. Ac., 85, 41–57, https://doi.org/10.1016/j.gca.2012.01.016, 2012.

765 Rundberg, Y. and Smalley, P. C.: High-resolution dating of Cenozoic sediments from northern North Sea using ^{87}Sr/^{86}Sr stratigraphy, Am. Assoc. Petrol. Geol. Bull., 73, 298–308, https://doi.org/10.1306/703C9B77-1707-11D7-8645000102C1865D, 1989.

Schaltegger, U., Stille, P., Rais, N., Pique, A., and Clauer, N.: Neodymium and strontium isotopic dating of diagenesis and low-grade metamorphism of argillaceous sediments, Geochim. Cosmochim. Ac., 58, 1471–1481, https://doi.org/10.1016/0016-7037(94)90550-9, 1994.

Schoneveld, L., Spandler, C., and Hussey, K.: Genesis of the central zone of the Nolans Bore rare earth element deposit, Northern Territory, Australia, Contrib. Mineral. Petrol., 170, 11, https://doi.org/10.1007/s00410-015-1168-x, 2015.

Schultz, J. L., Boles, J. R., and Tilton, G. R.: Tracking calcium in the San Joaquin basin, California: a strontium isotopic study of carbonate cements at North Coles Levee, Geochim. Cosmochim. Ac., 53, 1991–1999, https://doi.org/10.1016/0016-7037(89)90319-0, 1989.

Shewan, L. G., Armstrong, R. A., and O'Reilly, D.: Baseline bioavailable strontium isotope values for the investigation of residential mobility and resource-acquisition strategies in prehistoric Cambodia, Archaeom., 62, 810–826. https://doi.org/10.1111/arcm.12557, 2020.

Shields, G. A.: A normalised seawater strontium isotope curve and the Neoproterozoic-Cambrian chemical weathering event. eEarth Disc., 2, 69–84, https://hal.archives-ouvertes.fr/hal-00298250/document, 2007.

Shin, W.- J., Ryu, J.- S., Kim, R.- H., and Min, J.- S.: First strontium isotope map of groundwater in South Korea: applications for identifying the geographical origin, Geosci. J., 25, 173–181, https://doi.org/10.1007/s12303-020-0013-z, 2021.

Simandl, G. J. and Paradis, S.: Vanadium as a critical material: economic geology with emphasis on market and the main deposit types, Applied Earth Science, 131, 218–236, https://doi.org/10.1080/25726838.2022.2102883, 2022.

Smalley, P. C., Lønøy, A., and Råheim, A.: Spatial ^{87}Sr/^{86}Sr variations in formation water and calcite from the Ekofisk chalk oil field: implications for reservoir connectivity and fluid composition, Appl. Geochem., 7, 341–350, https://doi.org/10.1016/0883-2927(92)90024-W, 1992.

Smalley, P. C., Råheim, A., Rundberg, Y., and Johansen, H.: Strontium-isotope stratigraphy: applications in basin modelling and reservoir correlation. Chap. 3 in: Correlation in Hydrocarbon Exploration, Norwegian Petrol. Soc., Graham and Trotman, 23–31, https://doi.org/10.1007/978-94-009-1149-9_3, 1989.

Stueber, A. M., Pushkar, P., and Hetherington, E. A.: A strontium isotopic study of formation waters from the Illinois basin, U.S.A., Appl. Geochem., 2, 477–494, https://doi.org/10.1016/0883-2927(87)90003-5, 1987.

Sullivan, M. D., Haszeldine, R. S., and Fallick, A. E.: Linear coupling of carbon and strontium isotopes in Rotliegend Sandstone, North Sea: evidence for cross-formational fluid flow, Geology, 18, 1215–1218, https://doi.org/10.1130/0091-7613(1990)018%3C1215:LCOCAS%3E2.3.CO;2, 1990.

Swart, P. K., Ruiz, J., and Holmes, C. W.: Use of strontium isotopes to constrain the timing and mode of dolomitization of upper Cenozoic sediments in a core from San Salvador, Bahamas, Geology, 15, 262–265, https://doi.org/10.1130/0091-7613(1987)15%3C262:UOSITC%3E2.0.CO;2, 1987.

Tukey, J. W.: Exploratory Data Analysis, Addison-Wesley Publishing Company, Reading, MA, 506 pp., 1977.

Van Kranendonk, M. J., Hickman, A. H., Smithies, R. H., Nelson, D. R., and Pike, G.: Geology and tectonic evolution of the Archean North Pilbara Terrain, Pilbara Craton, Western Australia, Econ. Geol., 97, 695–732, https://doi.org/10.2113/gsecongeo.97.4.695, 2002.

Veizer, J.: Strontium isotopes in seawater trough time, Ann. Rev. Earth Planet. Sci., 17, 141–167, https://doi.org/10.1146/annurev.ea.17.050189.001041, 1989.

Vinciguerra, V., Stevenson, R., Pedneault, K., Poirer, A., Hélie, J.- F., and Widory, D.: Strontium isotope characterization of Wines from the Quebec (Canada) Terroir, Proc. Earth Planet. Sci., 13, 252–255, https://doi.org/10.1016/j.proeps.2015.07.059, 2015.

Voerkelius, S., Lorenz, G. D., Rummel, S., Quétel, C. R., Heiss, G., Baxter, M., Brach-Papa, C., Deters-Itzelsberger, P., Hoelzl, S., Hoogewerff, J., Ponzevera, E., Bocxstaele, M., and Van Ueckermann, H.: Strontium isotopic signatures of natural mineral waters, the reference to a simple geological map and its potential for authentication of food, Food Chem., 118, 933–940, https://doi.org/10.1016/j.foodchem.2009.04.125, 2010.

Vorster, C., Greeff, L., and Coetzee, P. P.: The determination of $^{11}B/^{10}B$ and $^{87}Sr/^{86}Sr$ isotope ratios by quadrupole-based ICP-MS for the fingerprinting of South African wine, South Afric. J. Chem., 63, 207–214, https://hdl.handle.net/10520/EJC24493, 2010.

Washburn, E., Nesbitt, J., Ibarra, B., Fehren-Schmitz, L., and Oelze, V. M.: A strontium isoscape for the Conchucos region of highland Peru and its application to Andean archaeology, PLOS ONE 16, e0248209, https://doi.org/10.1371/journal.pone.0248209, 2021.

Wei, C.- W., Xu, C., Chakhmouradian, A. R., Brenna, M., Kynicky, J., and Song, W.- L.: Carbon-strontium isotope decoupling in carbonatites from Caotan (Qinling, China): implications for the origin of calcite carbonatite in orogenic settings, J. Petrol., 61, egaa024, https://doi.org/10.1093/petrology/egaa024, 2020.

Wei, X., Wang, S., Ji, H., and Shi, Z.: Strontium isotopes reveal weathering processes in lateritic covers in southern China with implications for paleogeographic reconstructions, PLOS ONE, 13, e0191780, https://doi.org/10.1371/journal.pone.0191780, 2018.

Wickman, T. and Jacks, G.: Strontium isotopes in weathering budgeting. In: Water-Rock Interaction, Proc. 7th Int. Symp. Water-Rock Interaction (Park City, Utah, 13-18 July 1992), edited by: Kharaka, Y.K. and Maest, A.S., Balkema, Rotterdam, 1, 611–614, ISBN: 9054100753, 1992.

Wilford, J.: A weathering intensity index for the Australian continent using airborne gamma-ray spectrometry and digital terrain analysis, Geoderma, 183–184, 124–142, https://doi.org/10.1016/j.geoderma.2010.12.022, 2012.

Willmes, M., Bataille, C. P., James, H. F., Moffat, I., McMorrow, L., Kinsley, L., Armstrong, R.A., Eggins, S., and Grün, R.: Mapping of bioavailable strontium isotope ratios in France for archaeological provenance studies, Appl. Geochem., 90, 75–86, https://doi.org/10.1016/j.apgeochem.2017.12.025, 2018.

Willmes, M., McMorrow, L., Kinsley, L., Armstrong, R., Aubert, M., Eggins, S., Falguères, C., Maureille, B., Moffat, I., and Grün, R.: The IRHUM (Isotopic Reconstruction of Human Migration) database – bioavailable strontium isotope ratios for

835   geochemical fingerprinting in France, Earth Syst. Sci. Data, 6, 117–122, https://doi.org/10.5194/essd-6-117-2014, 2014.

Withnall, I. W., Hutton, L. J., Armit, R. J., Betts, P. G., Blewett, R. S., Champion, D. C., and Jell, P. A.: North Australian Craton. In: Geology of Queensland, edited by: Jell, P. A., Geol. Surv. Queensland, Brisbane, 23–112, ISBN: 9781921489761, https://www.business.qld.gov.au/industries/mining-energy-water/resources/geoscience-information/reports-news/geology-queensland-book-map (last access: 27 February 2023), 2013.

840   Wyborn, L. A. I., Heinrich, C. A., and Jaques, A. L.: Australian Proterozoic mineral systems: essential ingredients and mappable criteria, Austral. Inst. Mining Metall. (AusIMM) Ann. Conf. Proc. (Darwin, Northern Territory, 5-9 August 1994), 109–115, https://ecat.ga.gov.au/geonetwork/srv/api/records/a05f7892-f8a0-7506-e044-00144fdd4fa6 (last access: 27 February 2023), 1994.

Yang, C., Telmer, K., and Veizer, J.: Chemical dynamics of the "St. Lawrence" riverine system: δD_{H2O}, $\delta^{18}O_{H2O}$, $\delta^{13}C_{DIC}$,

845     $\delta^{34}S_{sulfate}$, and dissolved $^{87}Sr/^{86}Sr$, Geochim. Cosmochim. Ac., 60, 851–866, https://doi.org/10.1016/0016-7037(95)00445-9, 1996.

Zhao, Z., Leach, D. L., Wei, J., Liang, S., and Pfaff, K.: Origin of the Xitieshan Pb-Zn deposit, Qinghai, China: evidence from petrography and S-C-O-Sr isotope geochemistry, Ore Geol. Rev., 139A, 104429, https://doi.org/10.1016/j.oregeorev.2021.104429, 2021.